Global Biogeochemical Cycles

RESEARCH ARTICLE
10.1029/2021GB007202

Key Points:

- Global Nitrous oxide emissions increased from ~15.8 TgN/yr from the early 1990s to ~17.8 TgN/yr in the 2010s due to increasing anthropogenic sources
- Stratospheric enrichment contributes about +7.7‰/yr, +7.6‰/yr, +8.0‰/yr to the tropospheric $\delta^{15}N^{\alpha}$, $\delta^{15}N^{\beta}$, and $\delta^{18}O$ budget
- The 3-dimensional model estimated global mean isotopic signatures for anthropogenic sources are $\delta^{15}N{-}\alpha \sim -18‰$, $\delta^{15}N{-}\beta \sim -20‰$, and $\delta^{18}O \sim 19‰$

Supporting Information:

Supporting Information may be found in the online version of this article.

Correspondence to:

Q. Liang,
qing.liang@nasa.gov

Citation:

Liang, Q., Nevison, C., Dlugokencky, E., Hall, B. D., & Dutton, G. (2022). 3-D atmospheric modeling of the global budget of N_2O and its isotopologues for 1980–2019: The impact of anthropogenic emissions. *Global Biogeochemical Cycles*, *36*, e2021GB007202. https://doi.org/10.1029/2021GB007202

Received 21 SEP 2021
Accepted 22 JUN 2022

3-D Atmospheric Modeling of the Global Budget of N_2O and Its Isotopologues for 1980–2019: The Impact of Anthropogenic Emissions

Qing Liang[1], Cynthia Nevison[2], Ed Dlugokencky[3], Bradley D. Hall[3], and Geoff Dutton[3]

[1]NASA Goddard Space Flight Center, Atmospheric Chemistry and Dynamics Laboratory, Greenbelt, MD, USA, [2]University of Colorado, Institute of Arctic and Alpine Research, Boulder, CO, USA, [3]National Oceanic and Atmospheric Administration, Global Monitoring Laboratory, Boulder, CO, USA

Abstract Nitrous oxide (N_2O) is the third most important anthropogenic greenhouse gas and a major ozone-depleting substance. Its main sources include anthropogenic activities (mostly agriculture) and natural emissions from ocean and soils. However, emission estimates for individual sources are highly variable due to uncertainties in N_2O lifetime estimates and partitioning among sources. We derive annual global N_2O emissions for 1990–2019 using NOAA Global Monitoring Laboratory (GML) surface N_2O observations and the N_2O lifetime calculated in the NASA GEOS-5 chemistry climate model. The inferred global mean N_2O emissions has gradually increased from ~15.8 TgN/yr in the early 1990s to ~17.8 TgN/yr in the 2010s. This implies that anthropogenic N_2O emissions have grown rapidly from ~6.7 TgN/yr in the 1990s to about ~8.7 TgN/yr in the 2010s, a ~30% increase. With specially designed N_2O isotopic tracers in 3-D GEOSCCM, we estimate that, on global average, stratospheric enrichment contributes about +7.7‰/yr, +7.6‰/yr, +8.0‰/yr to tropospheric $\delta^{15}N^{\alpha}$, $\delta^{15}N^{\beta}$, and $\delta^{18}O$ budget, respectively. To balance the global mean isotopic signature for pre-industrial terrestrial sources of $\delta^{15}N^{\alpha} \sim 6.7‰$, $\delta^{15}N^{\beta} \sim -12.6‰$, $\delta^{18}O \sim 35.4‰$, our 3-dimensional isotopic budget simulation using the GEOSCCM suggests global mean anthropogenic isotopic signatures in the recent decades are $\delta^{15}N^{\alpha} \sim -18‰$, $\delta^{15}N^{\beta} \sim -20‰$, $\delta^{18}O \sim 19‰$. These anthropogenic isotopic estimates are significantly lighter than results from one-box atmospheric model-based estimates with the largest difference seen for $\delta^{15}N^{\beta}$. More surface isotopic measurements are needed to better quantify the N_2O isotopic signatures.

Plain Language Summary Nitrous oxide (N_2O) is a trace gas that plays an important role in Earth's atmosphere, impacting the chemical composition and radiation budget. In pre-industrial time, N_2O in the atmosphere primarily comes from ocean and soil emissions. Atmospheric N_2O level has increased by about 20% since mid 1800s as a result of human activities, mostly agriculture. Its growth rate in recent decades has been notably greater than before. Using a 3-Dimensional Chemistry Climate Model, we were able to determine that the notable increase in N_2O growth rate is a result of rapidly growing anthropogenic emissions started in the mid-1990s. In addition to the atmospheric mass balance budget of N_2O, we were also able to complete a full 3-Dimensional isotopic budget of ^{15}N and ^{18}O isotopologues for N_2O for 2000-2019 and estimated the contribution of isotopically-heavy stratospheric enrichment and isotopically-light anthropogenic sources. The increase in recent anthropogenic emissions has introduced detectable changes in the observed isotopic trends.

1. Introduction

Nitrous oxide (N_2O) is the third most important anthropogenic greenhouse gas (GHG), after carbon dioxide (CO_2) and methane (CH_4). N_2O is a long-lived gas with a best-estimate atmospheric lifetime of 123 years (SPARC, 2013) and a global warming potential that is ~300 times greater than CO_2 over a 100-year period (Forster et al., 2007). N_2O is also a major ozone-depleting substance (ODS) in the stratosphere (Ravishankara et al., 2009). Its main sources include anthropogenic activities (mostly agriculture) and natural emissions from ocean and soils. However, emissions from individual sources are highly uncertain. Due to increased emissions associated with human activities (Forster et al., 2007; Nevison et al., 2007; Park et al., 2012; Saikawa et al., 2014; Thompson et al., 2014), atmospheric N_2O has increased gradually from the pre-industrial 270 parts per billion (ppb) to about 332 ppb in 2019. The N_2O growth rate in recent decades has been notably greater than before, likely indicating rapidly growing anthropogenic emissions (Thompson et al., 2019; Tian et al., 2020). These changes highlight the

need for improved N_2O emission estimates of the present-day anthropogenic contribution and how it has evolved in the recent decades.

N_2O isotopologues increasingly have been used to investigate the magnitudes of N_2O sources and sinks (Frame et al., 2014; Park et al., 2011, 2012; Pérez et al., 2001). This is because N_2O from soil and oceanic sources and in stratospheric air have distinct isotopic signatures (Kim & Craig, 1990; Rahn & Wahlen, 2000; Yoshida & Toyoda, 2000), providing additional independent information to constrain the N_2O budget. It is well known that terrestrial N_2O sources contain relatively more of the lighter isotopologues than mean tropospheric background air (Park et al., 2011; Pérez et al., 2001), but the observed isotopologue signatures associated with soil fluxes are highly variable (Rahn & Wahlen, 2000). In contrast, the net isotopologue signature of oceanic N_2O sources remains a major unknown. This is because a wide range of isotopologue signatures has been reported for dissolved ocean N_2O, with some heavier and the others lighter than mean tropospheric N_2O (Kim & Craig, 1990). Rahn and Wahlen (2000) performed isotopic budget calculations assuming an isotopically "heavy", or alternatively "light", oceanic N_2O source, with respect to the tropospheric background. Subsequent studies generally have not advanced beyond this strategy with respect to the ocean. Snider et al. (2015) mined 1920 data points of in situ observations from 52 studies and reported the observed global mean $\delta^{15}N$ *is* ~6.63 ± 3.50 per mil (‰) and $\delta^{18}O \sim 47.34 \pm 9.54$‰ in the marine water samples. This suggests that marine water, distinctive from other sources, *e.g.*, freshwater, soil, or anthropogenic, has an isotopic signature close to the tropospheric background ($\delta^{15}N \sim 6.55 \pm 0.47$‰ and $\delta^{18}O \sim 44.4 \pm 0.34$‰) (Snider et al., 2015). In the stratosphere, the light N_2O isotopologue, $^{14}N^{14}N^{16}O$, is preferentially destroyed compared to the heavier isotopologues (Kim & Craig, 1990; Rahn & Wahlen, 1997; Yung & Miller, 1997). In the free troposphere, the light surface sources are balanced by the influx of isotopically enriched stratospheric air. As global N_2O emissions increase, the resulting atmospheric N_2O increase is accompanied by small decreases in the N_2O $\delta^{15}N$ and $\delta^{18}O$ isotopologue ratios (Ishijima et al., 2007; Park et al., 2012; Prokopiou et al., 2017; Röckmann et al., 2003; Röckmann & Levin, 2005; Toyoda et al., 2013). Overall, a comprehensive global database of N_2O isotopic measurements has yet to be compiled.

The observed background isotopic ratios for the three heavy isotopes, $\delta^{15}N^{\alpha}$ (the ^{15}N isotopic composition at the central nitrogen atom, the "α" site), $\delta^{15}N^{\beta}$ (the ^{15}N isotopic composition at the terminal nitrogen atom, the "β" site), and $\delta^{18}O$, have remained relatively stable, reflecting a close mass balance between the isotopically light surface sources and stratospheric enrichment. However, both N isotopomers show small but discernible negative trends, varying from −0.01 to −0.05‰/yr in the past decades, with an accompanying slight positive trend in site preference, $\delta^{15}N^{SP}$ (which equals to $\delta^{15}N^{\alpha} - \delta^{15}N^{\beta}$), of ~0.01‰/yr (Bernard et al., 2006; Ishijima et al., 2007; Park et al., 2012; Röckmann et al., 2003; Röckmann & Levin, 2005; Toyoda et al., 2013; Yu et al., 2020), likely indicating isotopic decrease in ^{15}N and ^{18}O abundances due to increased anthropogenic emissions and enhanced N fixation (Park et al., 2012). It is important to note that the observed $\delta^{15}N^{SP}$ trend has large uncertainties, mainly due to large uncertainties in $\delta^{15}N^{\beta}$ (Park et al., 2012; Prokopiou et al., 2017, 2018; Toyoda et al., 2013). The ^{18}O isotope has shown smaller negative trends, typically, −0.02‰/yr in the past decades (Bernard et al., 2006; Ishijima et al., 2007; Park et al., 2012; Röckmann et al., 2003; Röckmann & Levin, 2005), with three more recent studies even finding a small positive trend of +0.01‰/yr (Prokopiou et al., 2018; Toyoda et al., 2013; Yu et al., 2020). These ongoing trends, combined with the wide ranging and poorly known isotopic signatures of natural soil, freshwater, and oceanic sources, make it challenging to infer the isotopic signature of the anthropogenic source. There have been very limited 3-Dimensional (3D) chemical modeling studies of the N_2O isotopologues, likely due to high numerical precision needed for N_2O isotopic calculation that is exceedingly difficult for any tracer transport scheme (McLinden et al., 2003). The only comprehensive 3D modeling of full budget analysis of key N_2O isotopologues (McLinden et al., 2003) dates back almost two decades. McLinden et al. (2003) conducted a 3D chemical transport model calculation of mass flux balance between the stratospheric enrichment and surface sources and were able to reasonably reproduce the observed isotopic trends of $\delta^{15}N^{bulk}$, which equals to $(\delta^{15}N^{\alpha} + \delta^{15}N^{\beta})/2$, and $\delta^{18}O$ within 0.02‰/yr. However, McLinden et al. (2003) used relatively old measurements of N_2O isotopic fractionation for photolysis and $O(^1D)$ oxidation. More comprehensive isotopic fractionation measurements have become available since then (Hessberg et al., 2004; Kaiser et al., 2002b, 2002a, 2003; See Text S1 in Supporting Information S1 for more information). A recent study by Bernath et al. (2017) presented global distributions of $\delta^{15}N^{\alpha}$, $\delta^{15}N^{\beta}$, *and* $\delta^{18}O$ using the NCAR WACCM model and ACE-FTS satellite observations. However, this study used surface specified boundary conditions (with values of tropospheric air measured by Röckmann & Levin, 2005) and therefore unable to provide a free-running mass-balance budget calculation and trend analysis.

In this work, we use the NASA Goddard GEOS-5 chemistry climate model (CCM) to quantify the atmospheric budget of N_2O and its isotopes in recent decades. GEOSCCM is a comprehensive 3-D chemical model with realistic representation of stratospheric enrichment of the heavy isotopologues and credible subsequent atmospheric transport into the troposphere. As such it provides a novel tool for quantifying the contribution of stratospheric isotopic enrichment to the annual isotopic budget, and subsequently for inferring the contribution from surface emissions. We discuss in Section 3 the N_2O growth rate between 1980 and 2019, which reflects the balance between the rapidly increasing anthropogenic emissions and atmospheric N_2O photochemical destruction. We also use specially designed N_2O isotopic tracers to quantity the atmospheric isotopic budget of $\delta^{15}N$ and $\delta^{18}O$ for N_2O and the stratospheric enrichment contribution (Section 4). Through simultaneous simulation of N_2O and its isotopologues in a 3-dimensional (3-D) CCM framework, we analyze model simulated N_2O isotopic composition to examine the anthropogenic modification of the tropospheric N_2O isotopic signature (Section 4). Conclusions are presented in Section 5.

2. Modeling of N_2O and Its Isotopologues in the NASA GEOSCCM Model

2.1. Simulation of Atmospheric N_2O in GEOSCCM

The simulations presented in this study are conducted using the NASA GEOSCCM model (Nielsen et al., 2017), which couples the GEOS-5 model (Reinecker et al., 2008) with a detailed stratospheric chemistry module (Douglass et al., 2008). A comprehensive evaluation of several CCMs in previous multi-model assessments shows that the GEOSCCM simulation from 1960 to 2005 agrees well with observations for meteorological, transport-related, and chemical diagnostics (Dhomse et al., 2018; Eyring et al., 2006, 2007, 2010). GEOSCCM represents well the mean atmospheric circulation with realistic age-of-air and the simulated mean age of air from the N_2O runs (see below) is about 1.3 ± 0.3 years at 50 hPa in the tropics (20°S – 20°N) and about 3.9 ± 0.5 years in the polar middle stratosphere (50 hPa, >60°S/N), agreeing well with the observed CO_2-based estimates (Chipperfield et al., 2014). As the strength of the mean atmospheric circulation plays a key role in the atmospheric lifetime of the long-lived gases that are primarily destroyed in the stratosphere, this implies that GEOSCCM features realistic atmospheric, loss and hence atmospheric lifetime, for N_2O (Chipperfield et al., 2014). The model also features realistic inter-hemispheric transport, with an interhemispheric exchange time about 1.4 years, and reproduces well the observed differences of major long-lived halocarbons between the two hemispheres (Liang et al., 2008, 2014).

The GEOSCCM calculated mean N_2O lifetime (τ_{N2O}) against photolysis and $O(^1D)$ oxidation is about 117 ± 3 years for the present-day atmosphere. The model τ_{N2O} agrees well with the semi-empirical lifetime estimate of 116 ± 9 years from the Microwave Limb Sounder satellite measurements (Prather et al., 2015). The GEOSCCM τ_{N2O} and the SPARC (2013) multi-model mean τ_{N2O} (115 ± 9 years) are slightly shorter than the SPARC-recommended lifetime of 123 years. This is because the SPARC-recommended τ_{N2O} is derived using the average of model-based (115 ± 9 years), satellite-based (116 ± 21 years), and tracer-tracer-based (144 ± 23 years) estimates (SPARC, 2013). Therefore, the SPARC-recommended τ_{N2O} has a large uncertainty range of 104–152 years due to large observational uncertainties.

For this work, we conduct two GEOSCCM simulations: (a) a baseline simulation with constant global annual emissions of 15.5 TgN/yr, and (b) an optimized simulation with global total emissions varying between 15.2–18.3 TgN/yr and yields atmospheric N_2O growth rate that matches observations. In the baseline simulation, we use natural emissions of 9.1 TgN/yr from soil and ocean, following Prather et al. (2012, 2015), and constant global annual anthropogenic emissions of 6.4 TgN/yr for 1980–2019. These add up to global total N_2O emissions of 15.5 TgN/yr. The optimized simulation is driven with yearly varying anthropogenic emissions (6.1–9.2 TgN/yr) and global total emissions (15.2–18.3 TgN/yr) that are derived using the GEOSCCM-calculated N_2O lifetime and the surface-observation-inferred global N_2O annual mean atmospheric burden (see Section 3).

The oceanic emissions are from the observation-based oceanic emissions described in Nevison et al. (1995, 2004), but with an updated estimate calculated using surface winds from NCEP with improved spatially resolution. The better-resolved surface winds reduce global oceanic emissions to 2.5 TgN/yr. This updated oceanic emissions estimate agrees well with recent bottom-up estimates in Buitenhuis et al. (2018), who derived oceanic emissions from observed and model ΔpN_2O concentrations from two N_2O submodels (2.4 ± 0.8 and 2.5 ± 0.8 TgN/yr from these two submodel estimates). The estimated oceanic emissions using Bayesian inversion modeling approach

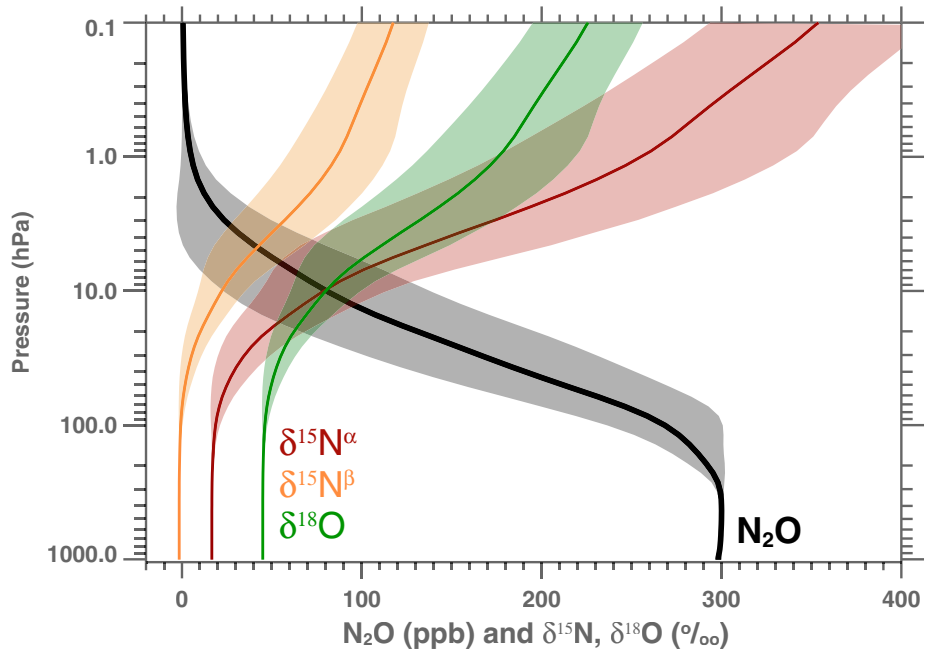

Figure 1. Annual averaged global mean vertical profiles of GEOSCCM simulated nitrous oxide (N_2O) (thick black line), $\delta^{15}N^{\alpha}$ (red line), $\delta^{15}N^{\beta}$ (orange line) and $\delta^{18}O$ (green line) for the year 2000. The corresponding color shadings are the 1-sigma variation of model simulated monthly mean values at all grids.

reported by Patra et al. (2022) is of similar magnitude, about 2.7 ± 0.3 TgN/yr. The soil emission distribution is from the monthly mean top-down estimates derived from the terrestrial biogeochemistry model described in Saikawa et al. (2013, 2014). Time and space-varying soil N_2O emissions were modeled by coupling the DNDC model of Li et al. (2000) to the Community Land Model (Saikawa et al., 2013). These emissions are scaled accordingly to yield a global natural soil source of 6.6 TgN/yr. The annual mean anthropogenic emissions distribution is from the EDGAR (Emission Database for Global Atmospheric Research) global inventory version 4.2 (http://edgar.jrc.ec.europa.eu/). These are dominated by agricultural sources, with additional small contributions from biomass burning (which is often associated with agriculture), industry, transportation, and energy emissions. The emission distribution of N_2O emissions from individual sources are shown in Figure S1 in Supporting Information S1.

2.2. Simulation of N_2O Isotopologues in GEOSCCM

In addition to the primary N_2O isotopologue, $^{14}N^{14}N^{16}O$, we include in GEOSCCM three heavier N_2O isotopologues, $^{14}N^{14}N^{18}O$, $^{14}N^{15}N^{16}O$, and $^{15}N^{14}N^{16}O$. All four isotopologues are transported individually in the model based on their molecular mixing ratios with respect to air density and maintain mass balance between surface emissions and photochemical destruction in the stratosphere. A detailed configuration of N_2O isotopic simulation and calculation is provided in Supplementary (Text S1 in Supporting Information S1).

Stratospheric photochemical destruction is the dominant enrichment process for N_2O isotopologues that balance the isotopically light surface sources. The global averaged annual mean vertical profiles of N_2O, $\delta^{15}N^{\alpha}$, $\delta^{15}N^{\beta}$, and $\delta^{18}O$ demonstrate that as N_2O decreases from ~300 ppb in the troposphere to near zero in the upper stratosphere, $\delta^{15}N^{\alpha}$, $\delta^{15}N^{\beta}$, and $\delta^{18}O$ increases rapidly because of stratospheric enrichment due to photolysis and $O(^1D)$ oxidation (Figure 1). The stratospheric enrichment is the strongest for $\delta^{15}N^{\alpha}$ and the weakest for $\delta^{15}N^{\beta}$, reflecting the differences in their associated isotopic fractionation in photolysis and $\boldsymbol{\varepsilon}$ values for the N_2O-$O(^1D)$ reaction. The model simulated scatter relationship of the N_2O isotopologue ratios of $\delta^{15}N^{bulk}$, $\delta^{15}N^{SP}$, *and* $\delta^{18}O$ versus N_2O mixing ratios and the vertical distribution of these isotopic signatures compare well with observations from previous balloon and aircraft measurements published in Rahn and Wahlen (1997), Park et al. (2004), and Toyoda et al. (2004); Figure 2. This indicates credible representation of the stratospheric isotopic fractionation

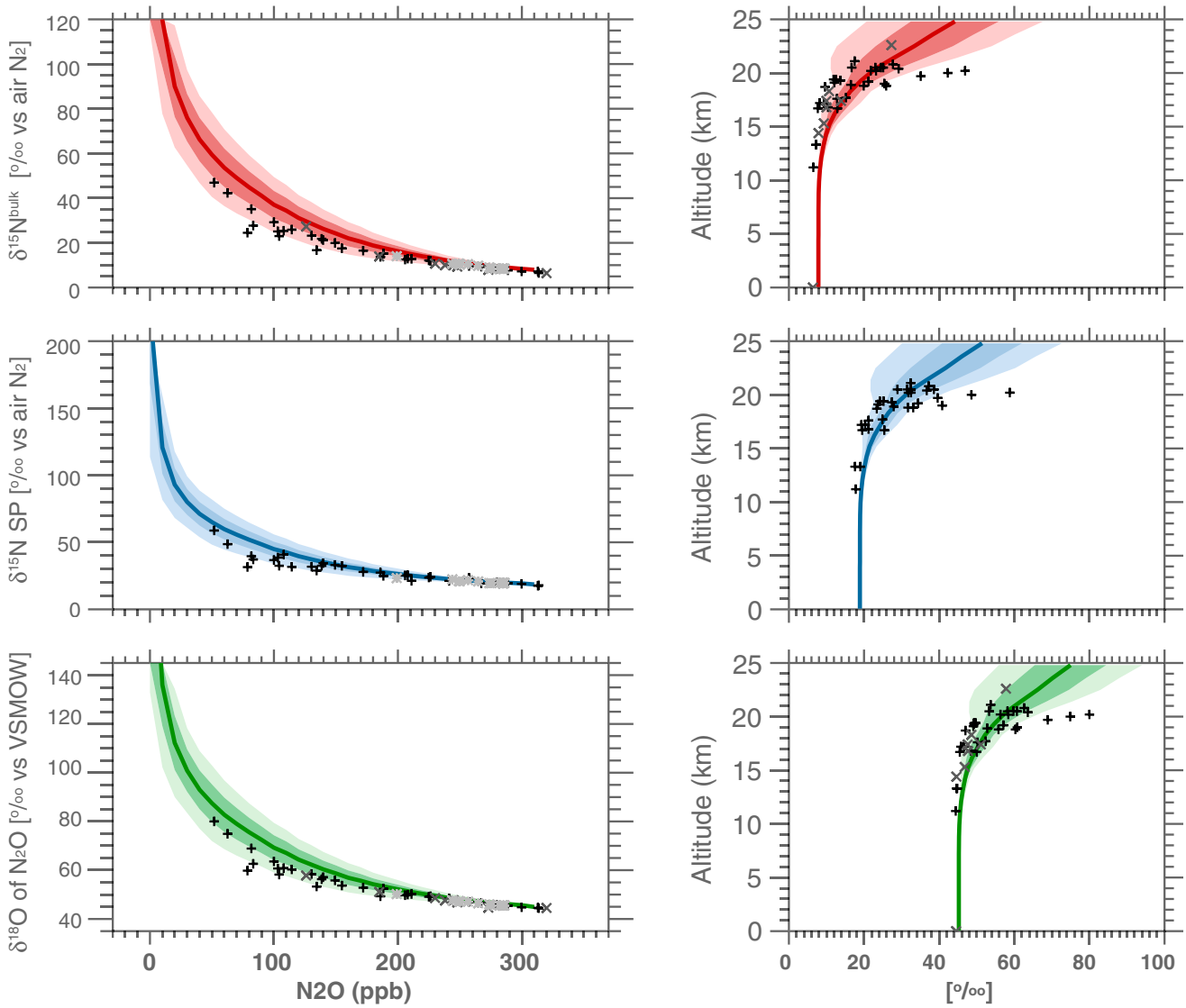

Figure 2. Comparison of GEOSCCM simulated $\delta^{15}N^{bulk}$ (top), $\delta^{15}N$ site preference (middle), and $\delta^{18}O$ (bottom) with observations collected in the upper troposphere and lower stratosphere (dark gray symbols for Rahn and Wahlen (1997); black symbols for Park et al. (2004); light gray symbols for Toyoda et al. (2004)). Both scatter relationship of isotopic ratios versus nitrous oxide (N_2O) (left column) and vertical distribution of isotopic ratios (right column) The thick solid color lines are model global averaged isotopologue ratios for the corresponding N_2O values. The corresponding dark and light color shadings show the model 1-sigma and 2-sigma ranges, respectively, calculated using model monthly mean output at all grids for January—December 2004. Note altitude information for the individual Toyoda et al. (2004) samples were not available, therefore not included on the right column plots.

in GEOSCCM. The spread of the isotopologue ratios with respect to a particular atmospheric N_2O abundance remains compact and does not change much with season or location in the atmosphere (Figure 2).

3. The Atmospheric N_2O Budget for 1980–2019

Observations made by the NOAA Global Monitoring Laboratory (GML) surface network in Hall et al. (2007) and Elkins and Dutton (2009) show that, although the annual growth rate displays large year-to-year variability due to measurements uncertainties prior to ~1995, global mean surface N_2O was rising steadily at an average rate of ~0.7 ppb/yr in the 1980s and 1990s (Figure 3ab). The N_2O growth rate has increased since the late-1990s and reaches an average of ~1.0 ppb/yr in the 2010s. This accelerated growth is also accompanied by a ~0.3 ppb increase in the observed N. Hemisphere—S. Hemisphere N_2O difference ($\Delta NH\text{-}SH_{N2O}$) (Figure 3c). The

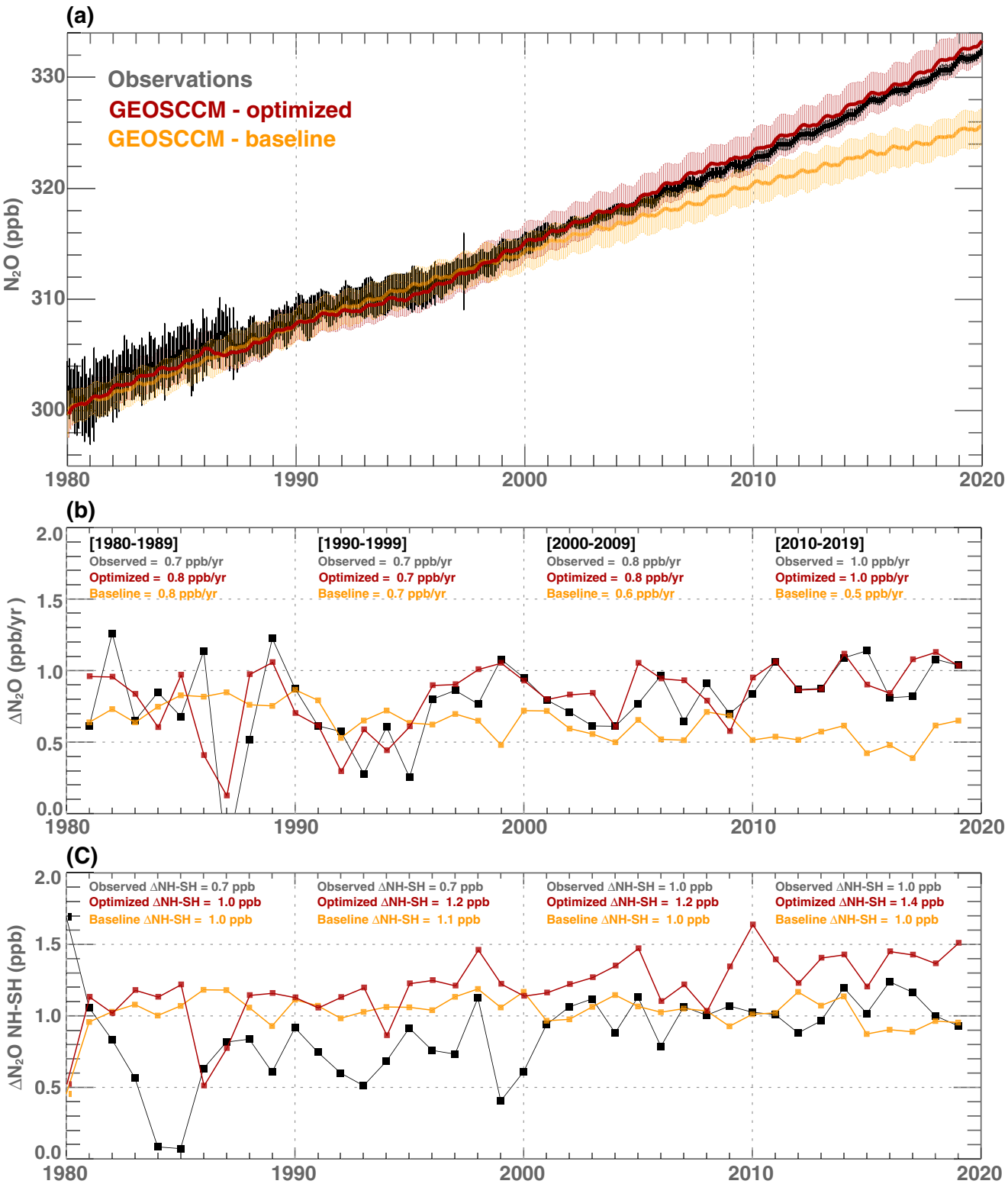

Figure 3. (a) GEOSCCM simulated global nitrous oxide (N_2O) (red line) versus NOAA Global Monitoring Laboratory (GML) observations (black line) using optimized global emissions, compared with results from the baseline simulation with a constant 15.5 TgN/yr (orange line). The vertical thin black lines show the uncertainty in GML estimated global mean N_2O. The vertical thin red and orange lines show the 1-sigma variations in model simulated surface N_2O in the corresponding simulations. (b) The comparison of GEOSCCM simulated annual growth rate (orange for baseline simulation and red for optimized simulation) and observed (black) growth rate. (c) Same as (b) but for annual averaged NH and SH molar fraction differences, $\Delta NH–SH_{N2O}$.

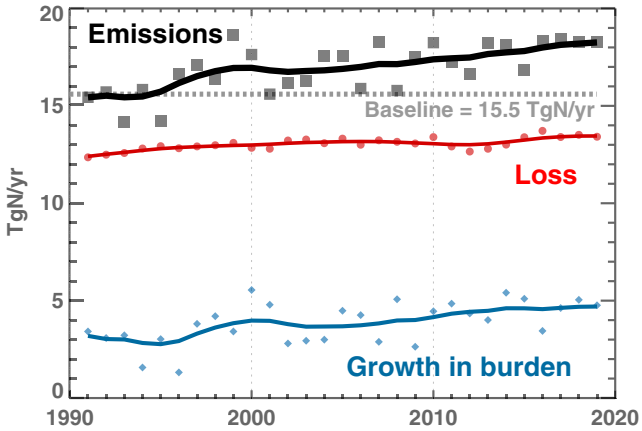

Figure 4. The GEOSCCM integrated annual atmospheric loss (red circles), atmospheric burden growth rate (blue diamonds), and global emissions (dark gray squares) for 1990—2019 from the optimized simulation. The annual emissions are inversely derived using the observed global mean nitrous oxide growth rate from NOAA Global Monitoring Laboratory surface network. The thick lines show the 10-year smoothed trends.

simultaneous increase in the growth rate and ΔNH-SH$_{N2O}$ implies that these changes are largely due to emissions increases in the NH.

The model global mean surface N_2O in the GEOSCCM baseline simulation agrees well with the observations between 1980 and 1999, but gradually deviates from the observations after 2000 (Figure 3a). Despite the constant annual emissions magnitude of 15.5 TgN/yr used to drive the simulation, the decadal average growth rate gradually decreases from ~0.7 ppb/yr in the 1980s to ~0.5 ppb/yr in the 2010s. This slowdown in model growth rate is mainly driven by faster atmospheric removal of N_2O due to a shorter N_2O lifetime (τ_{N2O}). The GEOSCCM calculated τ_{N2O} decreases slightly from 119 ± 2 years in the 1990s to 116 ± 2 years in 2010s with a corresponding increase in atmospheric loss at a rate ~0.4% per yr (+0.04 TgN per yr) (Figure 4). Recent multi-model analysis also reported a slight decrease of 6% from the 1960s to the 2000s (multiple-model mean decreased from 121 years in the 1980s to 118 years in the 2000s) in multi-model mean τ_{N2O}, with respect to a steady-state lifetime of 115 ± 9 years in 2000s (Chipperfield et al., 2014; SPARC, 2013). Patra et al. (2022) also reported a shortened τ_{N2O} of about 7 years from 1990 to 2019. The GEOSCCM simulated τ_{N2O} in the 2000s and 2010s in the optimized run is 1–2 years longer than the baseline run. This is because, due to the slow transport from surface to the upper atmosphere, rapidly increasing surface emissions led to a slightly out-of-balance atmosphere where upper atmospheric losses are lagging the relatively faster growth of atmospheric N_2O burden.

In this study, we conduct an atmospheric budget analysis of N_2O for 1990–2019, using the NOAA GML surface observations and the GEOSCCM corresponding atmospheric N_2O burden and loss for the year. The large variations in surface measurements in the 1980s (Hall et al., 2007; Elkins & Dutton, 2009) resulted in large uncertainties in the budget calculation. Therefore, here we limit our discussion on changes in global losses, emissions, and interhemispheric gradient to 1990–2019. The global emissions inferred from the observed growth rate have been rising in the recent decades (Figure 4). The accelerated growth in atmospheric burden is predominantly due to increasing emissions, with a small offset as a result of increasing loss. An averaged τ_{N2O} of about 117 ± 2 years corresponds to a mean atmospheric N_2O loss of 13.0 ± 0.3 TgN/yr for 1990–2019, with a slightly larger loss of 0.5 TgN/yr in the 2010s (mean loss of 13.2 ± 0.3 TgN/yr) as compared to the 1990s (mean loss of 12.7 ± 0.3 TgN/yr). The inferred global mean N_2O emissions gradually grows from ~15.5 TgN/yr in the early 1990s to an average emissions rate of 17.8 TgN/yr in the 2010s, with a mean growth rate of +0.1 TgN/yr. Assuming no significant changes in natural soil and oceanic emissions, this implies that anthropogenic emissions have increased from ~6.7 TgN/yr in early 1990s to ~8.7 TgN/yr in the 2010s, a 30% increase. While our inferred global mean N_2O emissions for 1998–2016 are comparable to the 17.0 (16.6–17.4) TgN/yr in Thompson et al. (2019), the inferred increase from 2000 to 2005 to 2010–2015 from GEOSCCM is ~0.8 TgN/yr, about half the derived increase of 1.6 TgN/yr in Thompson et al. (2019), as a result of changing lifetime in an interactive global CCM. Our inferred increase in anthropogenic emissions of ~1.8 TgN/yr from the 1990s to the 2010s is higher than the ~1.1 TgN/yr estimated in Tian et al. (2020). For a long-lived trace gas like N_2O that has a large atmospheric abundance, a change in lifetime of 1–2 years, albeit small, is not trivial in its budget calculation and emissions estimate. The origin of this lifetime difference can arise from a variety of reasons, *e.g.*, transient lifetime versus steady state lifetime especially during times when surface emissions change rapidly (as demonstrated by GEOSCCM simulations), the speedup of the circulation (Chipperfield et al., 2014), or year-to-year variability due to natural variability in atmospheric transport (Ray et al., 2020).

GEOSCCM does not simultaneously reproduce the observed growth rate and interhemispheric gradient ΔNH-SH$_{N2O.}$ While the optimized simulation, as expected, reproduces well the growth rate, the simulated ΔNH-SH$_{N2O}$ shows a systematic 0.3–0.5 ppb high bias compared to the observations, implying the emissions distribution used in the model is not correct. The modeled interhemispheric gradient is governed primarily by three factors, including interhemispheric transport timescale, NH-SH emission partition, and global emissions strength (e.g., Patra et al., 2011; Liang et al., 2014, 2017). Although the ΔNH-SH$_{N2O}$ from the baseline simulation

matches the observed ΔNH-SH$_{N2O}$, it merely reflects that the underestimate in NH-SH difference due to low-biased global emissions cancels off the high bias in the NH-SH difference due to high-biased NH-SH emission partition. Currently about 66% of total global emissions are from the NH in the GEOSCCM model, as 80% of the anthropogenic emissions are concentrated in the NH, particularly in the NH mid-latitudes (Figure S1). A significant fraction of the emissions needs to shift from the mid-latitude NH to the tropics or the SH to resolve the model bias. The recent NASA Atmospheric Tomography Mission (ATom) aircraft deployment mission (https://esdpubs.nasa.gov/pubs_by_mission/ATom) and the earlier NSF HIAPER Pole-to-Pole Observations (HIPPO) mission (Wofsy, 2011) provide latitudinally resolved pole-to-pole distribution of N_2O for four seasons. These measurements can be combined with 3-D chemical transport models in inversed modeling approaches to improve emissions and resolve some of the NH-SH gradient bias issue.

4. The Atmospheric Isotopic Budget of N_2O Between 1980 and 2019

4.1. Contribution of Stratospheric Enrichment

We design three idealized isotopologue tracers $^{15-\alpha}N_2O_{ST}$, $^{15-\beta}N_2O_{ST}$ and $N_2{}^{18}O_{ST}$ in GEOSCCM, in addition to the realistic N_2O isotopologues, to quantify the stratospheric enrichment of the minor isotopologues in the troposphere. These tagged isotopologues are initialized with the same atmospheric values as the realistic N_2O isotopologues at the beginning of the model simulation in January 1980. At the surface, the tagged tracers are modified by mixing with surface N_2O emissions that carry the same isotopic signatures as the observed mean tropospheric background; this configuration assumes all fresh surface emissions have the exact same fraction of $^{14}N^{14}N^{18}O$, $^{14}N^{15}N^{16}O$, $^{15}N^{14}N^{16}O$, and $^{14}N^{14}N^{16}O$ molecules as the tropospheric background. In the stratosphere, these tagged isotopologues go through stratospheric enrichment at the same rate as their corresponding ^{15}N and ^{18}O isotopologues. The differences between $^{15-\alpha}N_2O_{ST}$ versus $^{15-\alpha}N_2O$, $^{15-\beta}N_2O_{ST}$ versus $^{15-\beta}N_2O$, and $N_2{}^{18}O_{ST}$ versus $N_2{}^{18}O$ reflect the modification of the tropospheric mean isotopic signature due to stratospheric enrichment. These differences grow cumulatively throughout the model simulation years, reflecting the continuous addition of stratospheric enrichment.

During winter in each hemisphere, the descending branch of the Brewer-Dobson Circulation (BDC) transports stratospheric air that is depleted in N_2O and enriched with heavy isotopologues from the middle stratosphere into the troposphere. This downward transport is illustrated in Figure 5 for N_2O and $\delta^{18}O_{ST}$. The other two, $\delta^{15}N^{\alpha}{}_{ST}$ and $\delta^{15}N^{\beta}{}_{ST}$, have similar patterns, in terms of seasonality and magnitude, and are therefore not shown to avoid redundancy. After crossing the tropopause around spring, the negative N_2O and positive $\delta^{18}O_{ST}$ anomalies slowly propagate downward and reach the surface during late summer and early fall. This downward propagation of stratospheric air associated with the BDC and the ensuing stratosphere-troposphere exchange and its impact on long-lived gases, such as N_2O and CFCs, have been previously described in Nevison et al. (2004, 2011) and Liang et al. (2008, 2009). There is a hemispheric asymmetry in stratosphere-to-troposphere transport (STT) with stronger wave driving mixing rates and downward Brewer-Dobson stratospheric circulation in the NH (Appenzeller et al., 1996; Haynes et al., 1991; Holton et al., 1995). As a result, STT of isotopically enriched stratospheric air results in stronger seasonal cycles of $\delta^{15}N^{\alpha}{}_{ST}$, $\delta^{15}N^{\beta}{}_{ST}$, and $\delta^{18}O_{ST}$ in the NH than that in the SH (Figures 6 and 7).

These idealized isotopic ratios $\delta^{15}N^{\alpha}{}_{ST}$, $\delta^{15}N^{\beta}{}_{ST}$, and $\delta^{18}O_{ST}$ grow steadily at +7.74‰/yr, +7.62‰/yr, and +8.00‰/yr, respectively (Figure 6), when the input surface emissions were kept at the same isotopic signature as the present-day observed tropospheric value. These values provide global and annual averaged quantitative estimates of the stratospheric enrichment contribution to the tropospheric N_2O isotopic budget. Although the differences between the isotopologues are as large as 100–200‰ in the upper atmosphere (near 1 hPa), the differences between isotopologues near the surface are only a few tenths ‰. This likely reflects, in air mass exchange balance, air from the upper atmosphere that has very low density (0.1–10 hPa), when brought downward to mix with dense surface air (~1000 hPa), only exerts a small impact on the surface isotopic signature. On annual average, mean $\delta^{15}N^{\alpha}{}_{ST}$, $\delta^{15}N^{\beta}{}_{ST}$, and $\delta^{18}O_{ST}$ in the NH are ~0.3–~0.4‰ larger than those in the SH, implying a slightly larger stratospheric enrichment contribution to the NH troposphere. This is consistent with stronger NH STE downward flux of air into the troposphere than that in the SH. The amplitude of the seasonal cycles of $\delta^{15}N^{\alpha}{}_{ST}$, $\delta^{15}N^{\beta}{}_{ST}$, and $\delta^{18}O_{ST}$ are remarkable, ~4‰ in the NH and ~1‰ in the SH. This suggests that there are large seasonal variations in the contribution of stratospheric enrichment into the troposphere. STT downward influx of isotopically enriched air occurs predominantly in late winter to early spring and the influx slowly mixes

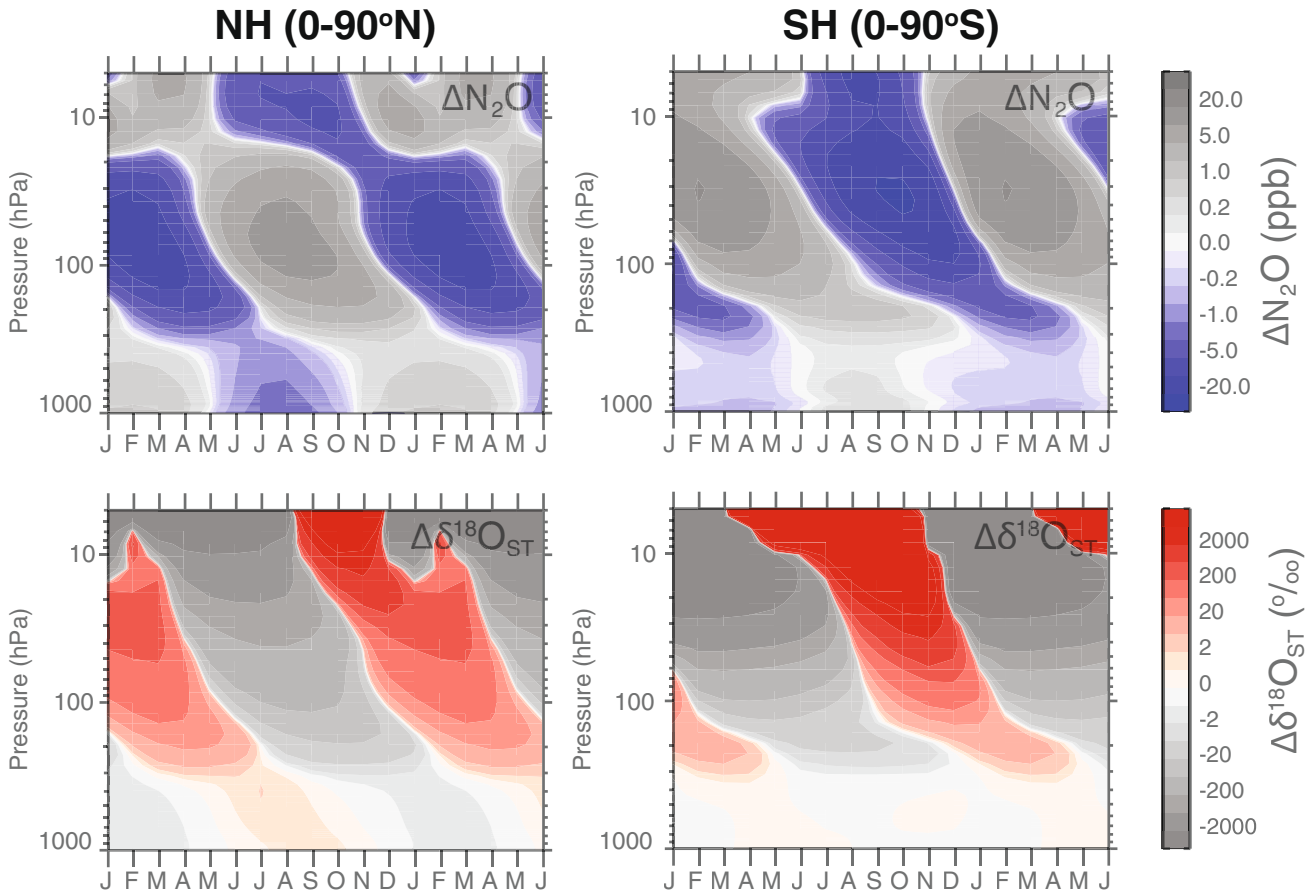

Figure 5. Seasonal evolution of NH (left) and SH (right) mean anomalous Nitrous oxide (N_2O) and $\Delta\delta^{18}O_{ST}$ showing the downward propagation of N_2O-depleted and isotopically enriched stratospheric air into the troposphere in the two hemispheres. The anomalies are calculated using the monthly averaged values at each grid using GEOSCCM output from 2000 to 2009.

downward, reaching the surface in late summer (Figure 6). Although the seasonal and interhemispheric variations are notable, the annual averaged $\delta^{15}N^{\alpha}_{ST}$, $\delta^{15}N^{\beta}_{ST}$, and $\delta^{18}O_{ST}$ in the troposphere around the globe grow at relatively the same rate, because of efficient hemispheric mixing in the troposphere and inter-hemispheric exchange with an exchange time scale of on the order of one year.

4.2. Box-Model Estimate of the Pre-Industrial Isotopic Budget

Several studies used box models with simplified assumptions about the impact of STE and conducted N_2O isotopic budget calculation (Ishijima et al., 2007; Park et al., 2012; Prokopiou et al., 2018; Röckmann et al., 2003; Snider et al., 2015; Yu et al., 2020). These studies provided a wide range of anthropogenic signatures, particularly for the $\delta^{15}N$ isotopomers. In this study, we follow a similar approach as the above studies and constructed a one-box model for the isotopic budget of N_2O. A detailed description of our one-box model is included in Text S2 in Supporting Information S1.

We apply our one-box model to the pre-industrial (PI) era using atmospheric N_2O abundance of 270 ppb and N_2O isotopic signatures of $\delta^{15}N^{\alpha} \sim 17.5 \pm 0.3‰$, $\delta^{15}N^{\beta} \sim 0.0 \pm 0.5‰$, $\delta^{18}O \sim 45.8–47.3‰$ measured from ice core and firn data (e.g., Bernard et al., 2006; Röckmann et al., 2003; Sowers et al., 2002). We estimate the global mean isotopic signatures for PI terrestrial sources are $\delta^{15}N^{\alpha} \sim 6.7‰$, $\delta^{15}N^{\beta} \sim -12.6‰$, $\delta^{18}O \sim 35.4‰$. The oceanic emissions of 2.5 TgN/yr used in this study is at the lower end of previous estimates of 3.4 ± 0.9 TgN/yr (Tian et al., 2020, and references therein). If we use oceanic emissions of 4.3 TgN/yr from the upper end, the inferred global mean isotopic signatures for PI terrestrial sources to balance the PI isotopic budget are significantly lighter ($\delta^{15}N^{\alpha} \sim 0.0‰$, $\delta^{15}N^{\beta} \sim -16.0‰$, $\delta^{18}O \sim 26.5‰$) because of smaller emissions.

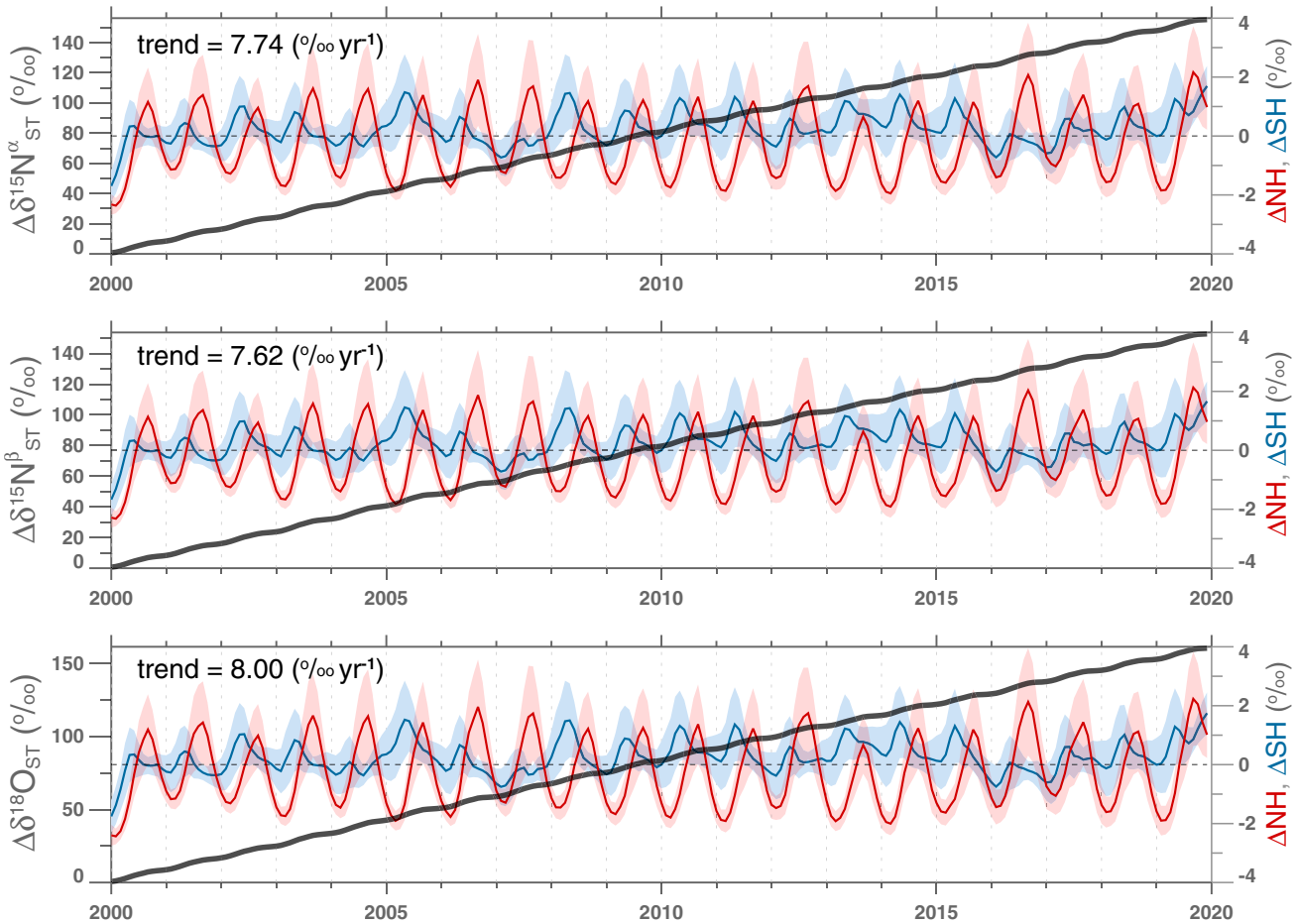

Figure 6. GEOSCCM simulated global average monthly mean $\Delta\delta^{15}N^{\alpha}_{ST}$, $\Delta\delta^{15}N^{\beta}_{ST}$, and $\Delta\delta^{18}O_{ST}$ (thick gray lines in each panel) at the surface, normalized as the absolute difference between the value of that month and the initial value in January 2000. Note that here we are only showing model results after 2000 after the tracers are fully spun-up with respect to the Brewer-Dobson circulation (in approximately 10–15 years). The deviation of hemispheric averaged $\delta^{15}N^{\alpha}_{ST}$, $\delta^{15}N^{\beta}_{ST}$, and $\delta^{18}O_{ST}$ in each month from the global mean values are also shown for the two hemispheres (red for NH and blue for SH, with shading indicating the 1-sigma variance at all surface grids in each hemisphere).

An isotopically balanced steady-state PI atmosphere implies the annual modification due to the addition of lighter surface sources must equal the stratospheric enrichment, which is dictated by the isotopic fractionation rate of photolysis and O(^{1}D) oxidation in the stratosphere. Note that the partition of emissions between soil and ocean does not alter the mean isotopic signatures for PI natural sources. Although our estimated $\delta^{15}N^{\beta} \sim -7.6‰$ for the PI natural emissions is very close to previous two-box model-based (one box for the troposphere and one box for the stratosphere) estimates (e.g., Park et al., 2012; Prokopiou et al., 2017, 2018), our estimated $\delta^{18}O \sim 38.0‰$ is somewhat heavier and our estimated $\delta^{15}N^{\alpha} \sim 9.8‰$ is considerably heavier than the derived values in these studies (Table 1). The estimated difference is largest for $\delta^{15}N^{\alpha}$, which features the steepest vertical gradient (Figure 1) in the stratosphere due to more efficient photochemical fractionation, and smallest for $\delta^{15}N^{\beta}$, which has the smallest vertical gradient. The differences between our study and previous estimates primarily reflect the different assumptions about the stratospheric enrichment contribution in the isotopic budget calculation. Park et al. (2012) and Prokopiou et al. (2017, 2018) adopted the same approach as Röckmann et al. (2003) and used the stratospheric enrichment factors of 21.3‰ for $\delta^{15}N^{\alpha}$, 12.9‰ for $\delta^{15}N^{\beta}$, and 14.0‰ for $\delta^{18}O$. These stratospheric enrichment contributions are estimated based on a few stratospheric air samples, therefore different from 3-D atmospheric model results derived using fully integrated global and annual mean flux into the troposphere.

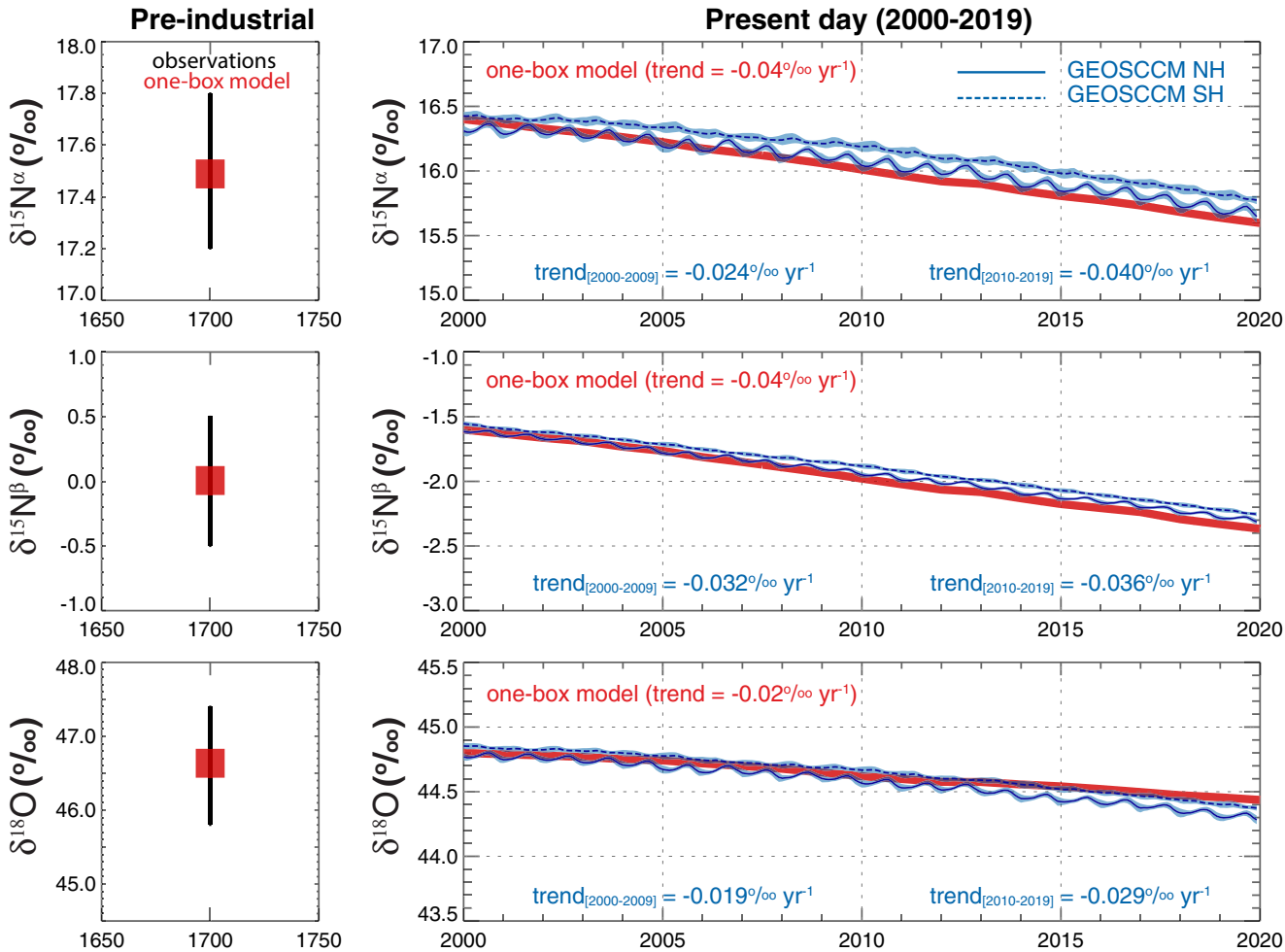

Figure 7. (Right) Monthly mean time series of $\delta^{15}N^{\alpha}$, $\delta^{15}N^{\beta}$, and $\delta^{18}O$ simulated by the one-box model (red lines) and the 3-D GEOSCCM model (blue solid lines for the NH mean and blue dashed lines for the SH mean; blue shading indicates one sigma variation in the near-surface grid cells in each hemisphere). The same one box model is used to estimate the isotopic signatures for natural soil emissions for the PI era that match the observed $\delta^{15}N^{\alpha}$, $\delta^{15}N^{\beta}$, and $\delta^{18}O$ values (left), as described in Section 4.1.

Table 1

Pre-Industrial and Present-Day Isotopic Budget of $\delta^{15}N$ and $\delta^{18}O$ Ratios for Natural Soil + Ocean N_2O Source Signatures From the One-Box Model and 3-Dimensional GEOSCCM Simulation in This Study, and Comparison to Previous Box Model Estimates for the Natural Background (Soils and Ocean)

	Tropospheric background	Stratos. Influx	Soils[a]	Natural (Soils + Ocean)	Park et al. (2012)	Prokopiou et al. (2017)	Prokopiou et al. (2018)
$\delta^{15}N^{\alpha}$ (‰)	17.5	25.2	6.7 (0.0)	9.8	−3.3 ± 1.0	−1.9 ± 1.0	−5.2 ± 0.4
$\delta^{15}N^{\beta}$ (‰)	0.0	7.6	−12.6 (−16.0)	−7.6	−7.5 ± 1.1	−8.3 ± 1.1	−7.5 ± 0.4
$\delta^{15}N^{bulk}$ (‰)	8.8	16.5	−3.0 (−8.0)	1.1	−5.3 ± 0.2	−5.2 ± 0.2	−6.8 ± 0.1
$\delta^{15}N^{SP}$ (‰)	17.5	17.6	19.3 (16.0)	19.6	4.2 ± 1.5	6.4 ± 1.5	2.3 ± 0.7
$\delta^{18}O$ (‰)	45.8–46.7	54.0	35.4 (26.5)	38.0	32.0 ± 0.2	33.1 ± 0.2	33.7 ± 0.2

Note. Note in this study, we assume ocean sources have the same isotopic signature as tropospheric background.

[a]These were derived using oceanic emissions of 2.5 TgN/yr and soil emissions of 6.6 TgN/yr. Estimates with the upper-end oceanic emissions of 4.3 TgN/yr and soil emissions of 4.8 TgN/yr are included in parenthesis.

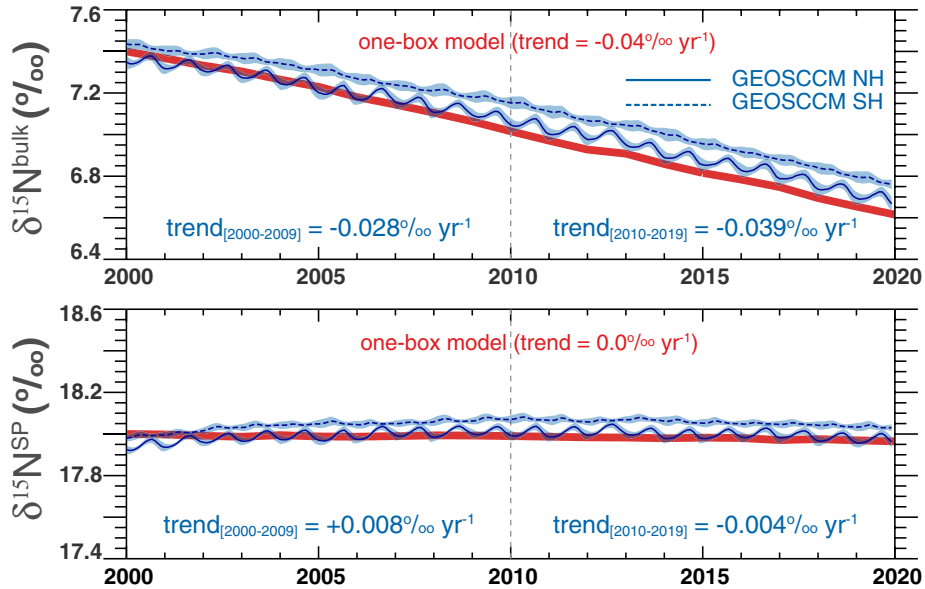

Figure 8. Same as Figure 7 right panel but for $\delta^{15}N^{bulk}$ and $\delta^{15}N^{SP}$, one-box model results in red and GEOSCCM results in blue.

4.3. Present-Day Isotopic Budget and the Impact of Growing Global Emissions

We use the observed mean tropospheric isotopic decline rates in the past few decades as primary constraints to infer the global mean isotopic signature for anthropogenic sources needed to reproduce these trends. For this study, for $\frac{\Delta R^X}{\Delta t}$, we use the average of the previously published observed isotopic trends: $\Delta\delta^{15}N^{\alpha} \sim -0.04$‰/yr, $\Delta\delta^{15}N^{\beta} \sim -0.04$‰/yr, $\Delta\delta^{18}O \sim -0.02$‰/yr (Ishijima et al., 2007; Park et al., 2012; Röckmann et al., 2003; Toyoda et al., 2013; Yu et al., 2020), as our observational constraints for long-term trends. The same isotopic budget calculation is performed with both the one-box model (Text S2 in Supporting Information S1) and the 3-D atmospheric chemistry transport model to assess the derived results. In the 3-D GEOSCCM simulation, since there is no realistic geographically resolved isotopic signature information available, for each isotopologue, we apply the same value at all locations to all molecules that are emitted to the atmosphere from the same emission source. Note that in the 3-D model calculation, while same isotopic budget calculation (Equation 5 in Text S2 in Supporting Information S1) is performed at all grid cells, the inferred anthropogenic isotopic signatures are estimated based on a globally integrated isotopic decline rate that matches the observations within ±0.01‰/yr. The integrated evolution of the tropospheric mean isotopic ratios $\delta^{15}N^{\alpha}$, $\delta^{15}N^{\beta}$, and $\delta^{18}O$ from both the one box-model and 3-D GEOSCCM simulation between 2000 and 2019 are shown in Figure 7. For easy comparison with reported observations, we have also shown the GEOSCCM simulated $\delta^{15}N^{bulk}$ and $\delta^{15}N^{SP}$ in Figure 8.

We use the one-box model and 3-D model, respectively, to calculate the modification due to stratospheric enrichment and natural emissions from soils and ocean and simulate the mass balance of each isotopologue. We find a set of optimized isotopic signatures for the anthropogenic sources which yields long-term trends that best match the observed trends. For our present-day isotopic one-box model, we infer that the global mean isotopic signatures for anthropogenic sources between 2000 and 2019 are $\delta^{15}N^{\alpha} \sim 1.7$‰, $\delta^{15}N^{\beta} \sim -14.9$ ‰, $\delta^{18}O \sim 33.2$‰. The 3-D GEOSCCM derived estimates ($\delta^{15}N^{\alpha} \sim -18$‰, $\delta^{15}N^{\beta} \sim -20$‰, $\delta^{18}O \sim 19$‰) are remarkably lighter than the one-box model estimates (Table 2). In addition, our sensitivity tests suggest that the simulated global mean isotopic ratios are highly sensitive to the assigned anthropogenic isotopic signatures; ±1–2‰ changes led to a noticeable change in the simulated mean trends, on the order of ~±0.01‰/yr. The three isotopologues have different sensitivities to per mil changes in the anthropogenic isotopic signature changes, with $\delta^{15}N^{\alpha}$ being the most sensitive and $\delta^{15}N^{\beta}$ being the least sensitive. Unlike the one-box model that shows a relatively constant rate of change in the simulated isotopic trends during the 20-year period, as anthropogenic emissions increase from 7.8 to 8.2 TgN/yr in the 2000s to 8.3–9.2 TgN/yr in the 2010s, the 3-D simulated results show noticeable larger decreasing trends in the 2010s, particularly for $\delta^{15}N^{\alpha}$ and $\delta^{18}O$. A 10-year sensitivity run (2010–2019)

Table 2
Present-Day (2000–2019) Isotopic Budget of $\delta^{15}N$ and $\delta^{18}O$ Ratios for Anthropogenic Nitrous Oxide (N_2O) Source Signatures From the Box Model and 3-Dimensional (3-D) GEOSCCM Simulation in This Study

	Tropo. BCG	Stratos. Influx	Anthropogenic		Sowers et al. (2002)	Ishijima et al. (2007)	Park et al. (2012)	Toyoda et al. (2013)	Prokopiou et al. (2017)	Prokopiou et al. (2018)	Yu et al. (2020)
			Box model	GEOSCCM							
$\delta^{15}N^{\alpha}$ (‰)	16.5	24.2	1.7 (3.4)	−18	–	NA	−7.6 ± 6.2	–	−8.1 ± 1.7	−4.5 ± 1.7	–
$\delta^{15}N^{\beta}$ (‰)	−1.5	6.1	−14.9 (−15.6)	−20	–	NA	−20.5 ± 7.1	–	−26.1 ± 8.4	−24.0 ± 8.4	–
$\delta^{15}N^{bulk}$ (‰)	7.5	15.2	−6.6 (−6.1)	−19	−7–−13	−11.6	−15.6 ± 1.2	−9.8 ± 1.0	−18.2 ± 2.6	−15.0 ± 2.6	−8.6 ± 4
$\delta^{15}N^{SP}$ (‰)	18	18.1	16.6 (19.0)	2	–	NA	13.1 ± 9.4	8.5 ± 7.8	18.0 ± 8.6	19.5 ± 8.6	10.7 ± 4
$\delta^{18}O$ (‰)	44.9	52.9	33.2 (36.3)	19	17–26	20–40	32.0 ± 1.3	36.0 ± 1.8	27.2 ± 2.6	30.0 ± 2.6	34.8 ± 3

Note. We also present a comparison of the derived mean isotopic signatures of anthropogenic sources to previous box model estimates.

using anthropogenic isotopic signatures from the one-box model calculation above yields a model-calculated tropospheric trend of $\Delta\delta^{15}N^{\alpha} \sim +0.07$‰/yr, $\Delta\delta^{15}N^{\beta} \sim -0.01$‰/yr, $\Delta\delta^{18}O \sim +0.04$‰/yr (not shown) and will not agree with the observed trends within the measurement uncertainty range. This implies that the differences of ∼6–20‰ between the one-box model and the 3-D model estimates cannot be reconciled easily by adjusting the input anthropogenic isotopic signatures.

Both the box model and 3-D model use the same N_2O budget information, *i.e.*, atmospheric burden, annual loss, and emissions, as well as the same isotopic signatures for each source and sink term. Hence, the most probable cause of the above differences is the inadequacy of a simple box-model in representing the complicated mixing process between the stratosphere and the troposphere, which is critical in the N_2O isotopic budget calculation. As illustrated in Section 4.1, the stratosphere-troposphere exchange shows distinctive seasonal variability and is stronger in the NH. In the meantime, the majority of the isotopically light anthropogenic emissions are released in the NH. With an interhemispheric exchange timescale >1 year, the isotopically lighter troposphere in the NH has a chance to first balance with the isotopically heavy stratospheric influx before it exchanges air with the SH troposphere, which is isotopically less variant because of less anthropogenic emissions and smaller stratospheric influx. This explanation is consistent with the GEOSCCM simulated variations in the hemispheric mean background isotopic ratios. The NH mean isotopic ratios, on annual average, are slightly lower than the SH mean due to more anthropogenic emissions at the surface but display much larger seasonal cycles (Figure 7). The amplitude of the NH seasonal cycles and the NH-SH difference are more pronounced in $\delta^{15}N^{\alpha}$ and $\delta^{18}O$, than those in $\delta^{15}N^{\beta}$ (Figures 7 and 9). This implies that $\delta^{15}N^{\beta}$ is less sensitive to STE influx and hence less susceptive to biases introduced due to the simplified transport representation in the one-box model.

The site preference of the ^{15}N isotopomers provides an effective means to constrain N_2O sources (Yoshida & Toyoda, 2000). However, it has been difficult to interpret the observed long-term trends of $\delta^{15}N^{SP}$ as they vary from positive values (Bernard et al., 2006; Park et al., 2012; Prokopiou et al., 2018; Röckmann & Levin, 2005; Yu et al., 2020) to negative values (Röckmann et al., 2003). The GEOSCCM result indicates that, by matching both the observed the $\delta^{15}N^{\alpha}$ and $\delta^{15}N^{\beta}$ trends, simulated $\delta^{15}N^{SP}$ remains relative constant at ∼18‰, but changes from a small positive trend to a small negative trend as anthropogenic emissions increase in the 2010s. This implies that $\delta^{15}N^{SP}$ trends can change signs as anthropogenic emissions change in magnitude. A better interpretation of the observed $\delta^{15}N^{SP}$ trends would need more accurate measurements of the isotopic signature of the anthropogenic sources as well as the magnitude of the anthropogenic emissions.

4.4. Comparison With Previous Isotopic Studies

We compare the results of our present-day one-box model estimate with previous published results and a detailed comparison is presented in Table 2. Note that most of the previous work uses a two-box model approach (one for the troposphere and one for the stratosphere) and account for the exchange of N_2O and its isotopologues between the troposphere and the stratosphere based on assumed mass exchange fluxes. The one-box approach we use here is equivalent to the two-box approach, but with the rate of troposphere-stratosphere mass exchange

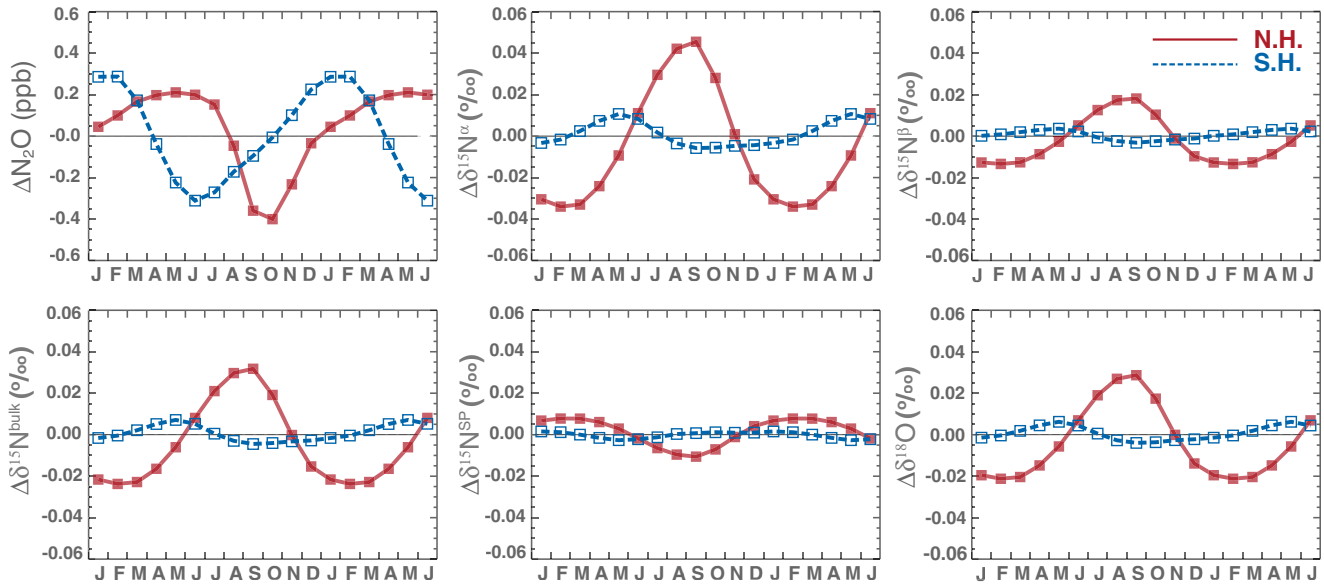

Figure 9. Seasonal cycle of anomalous near-surface (<1 km) Nitrous oxide (N_2O) and its isotopic ratios ($\delta^{15}N^{\alpha}$, $\delta^{15}N^{\beta}$, $\delta^{15}N^{bulk}$, $\delta^{15}N^{SP}$, and $\delta^{18}O$) averaged in the Northern Hemisphere (NH) and Southern Hemisphere (SH). These results are 20 years averages computed using the detrended GEOSCCM 2000–2019 results after detrending by applying a 13-month high-pass filter.

and the corresponding impacts being accounted for using the 3-D integrated stratospheric enrichment contribution term $Loss \times R^{X}_{strat}$. Our box model estimates of all isotopic signatures for present-day anthropogenic emissions are on the high-end of previous box model estimates (Ishijima et al., 2007; Park et al., 2012; Prokopiou et al., 2017, 2018; Sowers et al., 2002; Toyoda et al., 2013; Yu et al., 2020; Table 2, mostly due to a smaller stratospheric enrichment contribution. The 3-D model inferred estimates are on the lighter end of, or lighter than, the previous estimates, particularly for $\delta^{15}N^{\alpha}$ and $\delta^{18}O$ (Table 2). The 3-D model inferred $\delta^{15}N^{bulk}$ (−19‰), $\delta^{15}N^{SP}$ (2‰), and $\delta^{18}O$ (19‰) agree reasonably well with bottom-up estimates of isotopic composition from the majority of anthropogenic sources ($\delta^{15}N^{bulk} < -10$‰, $\delta^{15}N^{SP} < 10$‰, $\delta^{18}O < 30$‰) (Harris et al., 2017, and references therein).

The very low $\delta^{15}N^{SP}$ (2‰) for the anthropogenic sources, compared to previous box studies, is intriguing. This could stem from some of the simplification assumptions we made; for example, oceanic emissions have the same isotopic signature as the tropospheric background (hence $\delta^{15}N^{SP} \sim 18$‰). The magnitude of the natural soil and ocean emissions used in the 3-D modeling study can also impact our inferred estimates. Limited ocean observations showed that observed isotopologue signatures can vary from $\delta^{15}N^{SP} \sim 8$‰ in regions where there is N_2O production by nitrifier denitrification ($[O_2] > 5$ μM) to $\delta^{15}N^{SP} \sim 24$‰ in the N_2O consumption regions ($[O_2] < 5$ μM) (*e.g.*, Charpentier et al., 2007; Frame et al., 2014). Oceanic sources with lighter $\delta^{15}N^{SP}$, for example, <18‰, would have implied a larger $\delta^{15}N^{SP}$ value needed to balance the isotopic budget. In addition, the 3-D model is highly sensitive to changes in observed trend, the large uncertainties in the $\delta^{15}N^{SP}$ trend could also have impacted our results. Currently, surface and ocean isotopic measurements of N_2O isotopologues are extremely limited and more isotopic source signature samples are needed to advance our understanding of the N_2O isotopic budget. This is particularly true for $\delta^{15}N^{\beta}$ and/or $\delta^{15}N^{SP}$. More surface isotopic measurements over land and over the oceans, as well as bottom-up observational measurements of the isotopic composition near the primary source regions are needed to better constrain the N_2O isotopic budget.

In both the NH and SH, the N_2O isotopic ratios, $\delta^{15}N^{\alpha}$, $\delta^{15}N^{\beta}$, and $\delta^{18}O$, show an opposite seasonal cycle to that of N_2O, primarily driven by the seasonality of STE (Nevison et al., 2004, 2011; Park et al., 2012). As STE reaches maximum influence at the surface in late boreal summer in the NH and austral summer in the SH, model simulated N_2O is at its seasonal minimum and the isotopes at their seasonal maxima (Figure 9). $\delta^{15}N^{SP}$ shows a small but opposite seasonal cycle, due to the larger STE influence on $\delta^{15}N^{\alpha}$ than that on $\delta^{15}N^{\beta}$. Although it is not meaningful to compare our idealized model output to observations directly, a comparison of the amplitude of the modeled versus the observed seasonal cycle suggests that the GEOSCCM simulated seasonal variation

of $\delta^{15}N^{bulk}$ and $\delta^{18}O \sim \pm 0.03‰$ in the NH and $\sim \pm 0.01‰$ in the SH are on the same order of magnitude as the generally small and statistically insignificant seasonal cycles reported in the observations (Park et al., 2012; Toyoda et al., 2013; Yu et al., 2020). On the other hand, some studies observed larger seasonal cycles for selected isotopes, including $\delta^{15}N^{\alpha}$ (Park et al., 2012) and $\delta^{15}N^{SP}$ (Yu et al., 2020) with amplitudes on the order of $\sim \pm 0.4‰$, which is at least one magnitude larger in both hemispheres than the GEOSCCM model results. Further research is needed to determine whether these larger observed cycles are reproducible and statistically significant and, if so, are the seasonality of the ^{15}N isotopomers mostly related to surface emissions or to the stratospheric signal.

5. Conclusions

The atmospheric N_2O mixing ratio has been increasing at a faster rate in recent decades, likely indicating rapidly growing anthropogenic emissions. In this study, we used the NASA Goddard GEOS-5 chemistry climate model (CCM) to simulate N_2O and its isotopes between 1980 and 2019, to assess how anthropogenic emissions have impacted the atmospheric budget of N_2O and its isotopic composition in the present-day atmosphere.

Surface observations from the NOAA's Global Monitoring Laboratory (GML) surface network show that the N_2O growth rate increased from the ~0.7 ppb/yr in the 1980s and 1990s to an average of ~1.0 ppb/yr in the 2010s. This accelerated growth rate is also accompanied by a ~0.3 ppb increase in the observed Northern Hemisphere (NH)—Southern Hemisphere (SH) N_2O difference, implying that these changes are largely due to emissions increases in the NH. Our 3-D model-based budget analysis as constrained by the observed N_2O growth rate from the NOAA GML surface network suggests that global mean N_2O emissions remain relatively steady at ~15.8 TgN/yr from the early 1990s and gradually increases to an average rate of ~17.8 TgN/yr in the 2010s. This implies that anthropogenic emissions have increased from ~6.7 TgN/yr from the early 1990s to ~8.7 TgN/yr in the 2010s, ~30% increase.

On the isotopic side, using special designed isotopologue tracers in GEOSCCM, we demonstrated that, on annual average, the stratosphere-to-troposphere transport of isotopically heavy air contribute +7.7‰/yr, +7.6‰/yr, and +8.0‰/yr to the tropospheric $\delta^{15}N^{\alpha}$, $\delta^{15}N^{\beta}$, and $\delta^{18}O$, respectively. However, the stratospheric isotopic contributions show remarkable seasonal variation, ~4‰ in the NH and ~1‰ in the SH for all three isotopologues, and the annually averaged impact is slightly larger (~0.3 − ~0.4‰) in the NH than that in the SH. Using the observed isotopic trends observations ($-\Delta\delta^{15}N^{\alpha} \sim -0.04‰$/yr, $\Delta\delta^{15}N^{\beta} \sim -0.04‰$/yr, $\Delta\delta^{18}O \sim -0.02‰$/yr) as primary constraints in our 3-D atmospheric isotopic budget calculation, GEOSCCM estimated the global mean isotopic signatures of the anthropogenic emissions are: $\delta^{15}N^{\alpha} \sim -18‰$, $\delta^{15}N^{\beta} \sim -20‰$, $\delta^{18}O \sim 19‰$. These estimates are significantly lighter than our box-model estimates which were constructed using the same input of N_2O budget terms and the isotopic signatures for the stratospheric flux and natural emission sources as the 3-D model. The 3-D model-based estimates are also notably lighter/smaller than previously published box-model estimates, especially for $\delta^{15}N^{\alpha}$, $\delta^{18}O$, and $\delta^{15}N^{SP}$. The intriguing differences between the 3-D model estimate and the box-model estimate may suggest that realistic representation of the stratosphere-to-troposphere flux in each hemisphere and on a month-to-month timescale is an important process for N_2O isotopic budget calculation. Compared to the box-model, the 3-D model simulation also shows much higher sensitivity to the isotopic signatures used in budget calculation and observed trends. These differences highlight the need for more surface observations of the N_2O isotopic compositions over land and over the oceans, as well as bottom-up observational measurements of the isotopic composition near the primary source regions are needed to better constrain the N_2O isotopic budget, especially the ^{15}N isotopomers.

Data Availability Statement

NOAA GML measurements are available for public access at https://gml.noaa.gov/aftp/data/hats/n2o/combined/. The version of GEOSCCM model used in this study is described by Nielsen et al. (2017), https://doi.org/10.1002/2017ms001011 and information on N_2O isotopic related calculation is described in Text S1 in Supporting Information S1. Results from the GEOSCCM model simulations used in this study are available from the corresponding author, QL, upon request.

Acknowledgments
The authors thank the reviewers for their thoughtful comments and suggestions. This work was supported by NASA's Modeling, Analysis, and Prediction Program. GEOSCCM model description, configuration, input parameters and forcing datasets, and associated references are provided in Section 2 of the main text and the Supplementary (Text S1 in Supporting Information S1). Supercomputing resources for GEOSCCM were provided by the NASA High-End Computing (HEC) Program through the Advanced Supercomputing (NAS) Facility and NASA Center for Climate Simulation (NCCS).

References

Appenzeller, C., Holton, J. R., & Rosenlof, K. H. (1996). Seasonal variation of mass transport across the tropopause. *Journal of Geophysical Research: Atmospheres*, *101*, 15071–15078. https://doi.org/10.1029/96JD00821

Bernard, S., Röckmann, T., Kaiser, J., Barnola, J.-M., Fischer, H., Blunier, T., & Chappellaz, J. (2006). Constraints on N_2O budget changes since pre-industrial time from new firn air and ice core isotope measurements. *Atmospheric Chemistry and Physics*, *6*, 493–503. https://doi.org/10.5194/acp-6-493-2006

Bernath, P. F., Yousefi, M., Buzan, E., & Boone, C. D. (2017). A near-global atmospheric distribution of N_2O isotopologues. *Geophysical Research Letters*, *44*, 10735–10743. https://doi.org/10.1002/2017GL075122

Buitenhuis, E. T., Suntharalingam, P., & Le Quéré, C. (2018). Constraints on global oceanic emissions of N_2O from observations and models. *Biogeosciences*, *15*, 2161–2175. https://doi.org/10.5194/bg-15-2161-2018

Charpentier, J., Farias, L., Yoshida, N., Boontanon, N., & Raimbault, P. (2007). Nitrous oxide distribution and its origin in the central and eastern South Pacific Subtropical Gyre. *Biogeosciences*, *4*, 729–741. https://doi.org/10.5194/bg-4-729-2007

Chipperfield, M. P., Liang, Q., Strahan, S. E., Morgenstern, O., Dhomse, S. S., Abraham, N. L., et al. (2014). Multi-model estimates of atmospheric lifetimes of long-lived Ozone-Depleting-Substances: Present and future. *Journal of Geophysical Research: Atmospheres*, *119*, https://doi.org/10.1002/2013jd021097

Dhomse, S. S., Kinnison, D., Chipperfield, M. P., Salawitch, R. J., Cionni, I., & Hegglin, M. I. (2018). Estimates of ozone return dates from chemistry-climate model initiative simulations. *Atmospheric Chemistry and Physics*, *18*(11), 8409–8438. https://doi.org/10.5194/acp-18-8409-2018

Douglass, A. R., Stolarski, R. S., Schoeberl, M. R., Jackman, C. H., Gupta, M. L., Newman, P. A., et al. (2008). Relationship of loss, mean age of air and the distribution of CFCs to stratospheric circulation and implications for atmospheric lifetimes. *Journal of Geophysical Research: Atmospheres*, *113*, D14309. https://doi.org/10.1029/2007JD009575

Elkins, J. W., & Dutton, G. S. (2009). Nitrous oxide and sulfur hexafluoride in 'State of the Climate in 2008. *Bulletin of the American Meteorological Society*, *90*, S38–S39. https://doi.org/10.1175/BAMS-90-8-StateoftheClimate

Eyring, V., Butchart, N., Waugh, D. W., Akiyoshi, H., Austin, J., Bekki, S., et al. (2006). Assessment of temperature, trace species, and ozone in chemistry-climate model simulations of the recent past. *Journal of Geophysical Research: Atmospheres*, *111*, D22308. https://doi.org/10.1029/2006JD007327

Eyring, V., Cionni, I., Bodeker, G. E., Charlton-Perez, A. J., Kinnison, D. E., Scinocca, J. F., et al. (2010). Multi-model assessment of stratospheric ozone return dates and ozone recovery in CCMVal-2 models. *Atmospheric Chemistry and Physics*, *10*, 9451–9472. https://doi.org/10.5194/acp-10-9451-2010

Eyring, V., Waugh, D. W., Bodeker, G. E., Cordero, E., Akiyoshi, H., Austin, J., et al. (2007). Multimodel projections of stratospheric ozone in the 21st century. *Journal of Geophysical Research: Atmospheres*, *112*, D16303. https://doi.org/10.1029/2006JD008332

Forster, P., Ramaswamy, V., Artaxo, P., Berntsen, T., Betts, R., Fahey, D. W., et al. (2007). Changes in Atmospheric Constituents and in Radiative Forcing. In *Climate Change 2007: The Physical Science Basis. Contribution of Working Group I to the Fourth Assessment Report of the Intergovernmental Panel on Climate Change*. Cambridge University Press Cambridge.

Frame, C. H., Deal, E., Nevison, C. D., & Casciotti, K. L. (2014). N_2O production in the eastern South Atlantic: Analysis of N_2O stable isotopic and concentration data. *Global Biogeochemical Cycles*, *28*, 1262–1278. https://doi.org/10.1002/2013GB004790

Hall, B. D., Dutton, G. S., & Elkins, J. W. (2007). The NOAA nitrous oxide standard scale for atmospheric observations. *Journal of Geophysical Research: Atmospheres*, *112*, D09305. https://doi.org/10.1029/2006JD007954

Harris, E., Ibraim, E., Henne, S., Hüglin, C., Zellweger, C., Tuzson, B., et al. (2017). Tracking nitrous oxide emission processes at a suburban site with semicontinuous, in situ measurements of isotopic composition. *Journal of Geophysical Research: Atmospheres*, *122*, 1850–1870. https://doi.org/10.1002/2016JD025906

Haynes, P. H., McIntyre, M. E., Sheperd, T. G., Marks, C. J., & Shine, K. P. (1991). On the "downward control" principle of extratropical circulations by eddy-induced mean zonal forces. *Journal of the Atmospheric Sciences*, *48*, 651–678. https://doi.org/10.1175/1520-0469(1991)048<0651:otcoed>2.0.co;2

Hessberg, P., Kaiser, J., Enghoff, M. B., McLinden, C. A., Röckmann, S. L. S. T., & Johnson, M. S. (2004). Ultra-violet absorption cross sections of isotopically substituted nitrous oxide species $^{14}N^{14}NO$, $^{15}N^{14}NO$, $^{14}N^{15}NO$ and $^{15}N^{15}NO$. *Atmospheric Chemistry and Physics*, *4*, 1237–1253. https://doi.org/10.5194/acp-4-1237-2004

Holton, J. R., Haynes, P. H., McIntyre, M. E., Douglass, A. R., Rood, R. B., & Pfister, L. (1995). Stratosphere-troposphere exchange. *Review of Geophysics*, *33*(4), 403–439. https://doi.org/10.1029/95RG02097

Ishijima, K., Sugawara, S., Kawamura, K., Hashida, G., Morimoto, S., Murayama, S., et al. (2007). Temporal variations of the atmospheric nitrous oxide concentration and its $\delta^{15}N$ and $\delta^{18}O$ for the latter half of the 20th century reconstructed from firn air analyses. *Journal of Geophysical Research: Atmospheres*, *112*, D03305. https://doi.org/10.1029/2006JD007208

Kaiser, J., Brenninkmeijer, C. A. M., & Röckmann, T. (2002a). Intramolecular ^{15}N and ^{18}O fractionation in the reaction of N_2O with $O(^1D)$ and its implications for the stratospheric N_2O isotope signature. *Journal of Geophysical Research: Atmospheres*, *107*(D14), https://doi.org/10.1029/2001JD001506

Kaiser, J., Brenninkmeijer, C. A. M., & Röckmann, T. (2002b). Temperature dependence of isotopologue fractionation in N_2O photolysis. *Physical Chemistry Chemical Physics*, *4*. https://doi.org/10.1039/b204837j

Kaiser, J., Röckmann, T., Brenninkmeijer, C. A. M., & Crutzen, P. J. (2003). Wavelength dependence of isotope fractionation in N_2O photolysis. *Atmospheric Chemistry and Physics*, *3*, 303–313. https://doi.org/10.5194/acp-3-303-2003

Kim, K.-R., & Craig, H. (1990). Two-isotope characterization of N_2O in the Pacific Ocean and constraints on its origin in deep water. *Nature*, *347*, 58–61. https://doi.org/10.1038/347058a0

Li, C., Aber, J., Stange, F., Butterbach-Bahl, K., & Papen, H. (2000). A process-oriented model of N_2O and NO emissions from forest soils: 1. Model development. *Journal of Geophysical Research: Atmospheres*, *105*(D4), 4369–4384. https://doi.org/10.1029/1999JD900949

Liang, Q., Chipperfield, M. P., Fleming, E. L., Abraham, N. L., Braesicke, P., Burkholder, J. B., et al. (2017). Deriving global OH abundance and atmospheric lifetimes for long-lived gases: A search for CH3CCl3 alternatives. *Journal of Geophysical Research: Atmospheres*, *122*, 11914–11933. https://doi.org/10.1002/2017JD026926

Liang, Q., Douglass, A. R., Duncan, B. N., Stolarski, R. S., & Witte, J. C. (2009). The governing processes and timescales of stratosphere-to-troposphere transport and its contribution to ozone in the Arctic troposphere. *Atmospheric Chemistry and Physics*, *9*, 3011–3025. https://doi.org/10.5194/acp-9-3011-2009

Liang, Q., Newman, P. A., Daniel, J. S., Reimann, S., Hall, B. D., Dutton, G., & Kuijpers, L. J. M. (2014). Constraining the carbon tetrachloride (CCl_4) budget using its global trend and inter-hemispheric gradient. *Geophysical Research Letters*, *41*, 5307–5315. https://doi.org/10.1002/2014GL060754

Liang, Q., Stolarski, R. S., Douglass, A. R., Newman, P. A., & Nielsen, J. E. (2008). Evaluation of emissions and transport of CFCs using surface observations and their seasonal cycles and simulation of the GEOS CCM with emissions-based forcing. *Journal of Geophysical Research: Atmospheres*, *113*, D14302. https://doi.org/10.1029/2007JD009617

McLinden, C. A., Prather, M. J., & Johnson, M. S. (2003). Global modeling of the isotopic analogues of N_2O: Stratospheric distributions, budgets, and the ^{17}O–^{18}O mass-independent anomaly. *Journal of Geophysical Research*, *108*, 4233. https://doi.org/10.1029/2002JD002560

Nevison, C. D., Dlugokencky, E., Dutton, G., Elkins, J. W., Fraser, P., Hall, B., et al. (2011). Exploring causes of interannual variability in the seasonal cycles of tropospheric nitrous oxide. *Atmospheric Chemistry and Physics*, *11*, https://doi.org/10.5194/acp-11-3713-2011

Nevison, C. D., Lueker, T. J., & Weiss, R. F. (2004). Quantifying the nitrous oxide source from coastal upwelling. *Global Biogeochemical Cycles*, *18*, https://doi.org/10.1029/2003GB002110

Nevison, C. D., Mahowald, N. M., Weiss, R. F., & Prinn, R. G. (2007). Interannual and seasonal variability in atmospheric N_2O. *Global Biogeochemical Cycles*, *21*, GB3017. https://doi.org/10.1029/2006GB002755

Nevison, C. D., Weiss, R. F., & Erickson, D. J. III. (1995). Global oceanic emissions of nitrous oxide. *Journal of Geophysical Research: Atmospheres*, *100*, 15809–15820. https://doi.org/10.1029/95JC00684

Nielsen, J. E., Pawson, S., Molod, A., Auer, B., da Silva, A. M., Douglass, A. R., et al. (2017). Chemical mechanisms and their applications in the Goddard Earth Observing System (GEOS) Earth system model. *Journal of Advances in Modeling Earth Systems*, *9*(8), 3019–3044. https://doi.org/10.1002/2017MS001011

Park, S., Atlas, E. L., & Boering, K. A. (2004). Measurements of N_2O isotopologues in the stratosphere: Influence of transport on the apparent enrichment factors and the isotopologue fluxes to the troposphere. *Journal of Geophysical Research: Atmospheres*, *109*, D01305. https://doi.org/10.1029/2003JD003731

Park, S., Croteau, P., Boering, K., Etheridge, D. M., Ferretti, D., Fraser, P. J., et al. (2012). Trends and seasonal cycles in the isotopic composition of nitrous oxide since 1940. *Nature Geoscience*, *5*, 261–265. https://doi.org/10.1038/ngeo1421

Park, S., Perez, T., Boering, K. A., Trumbore, S. E., Gil, J., Marquina, S., & Tyler, S. C. (2011). Can N_2O stable isotopes and isotopomers be useful tools to characterize sources and microbial pathways of N_2O production and consumption in tropical soils? *Global Biogeochemical Cycles*, *25*, https://doi.org/10.1029/2009GB003615

Patra, P. K., Dlugokencky, E. J., Elkins, J. W., Dutton, G. S., Tohjima, Y., Sasakawa, M., et al. (2022). Forward and inverse modelling of atmospheric nitrous oxide using MIROC4-atmospheric chemistry-transport model. *Journal of the Meteorological Society of Japan. Ser. II*. https://doi.org/10.2151/jmsj.2022-018

Patra, P. K., Houweling, S., Krol, M., Bousquet, P., Belikov, D., Bergmann, D., et al. (2011). TransCom model simulations of CH_4 and related species: Linking transport, surface flux and chemical loss with CH_4 variability in the troposphere and lower stratosphere. *Atmospheric Chemistry and Physics*, *11*, 12813–12837. https://doi.org/10.5194/acp-11-12813-2011

Pérez, T., Trumbore, S. E., Tyler, S. C., Matson, P. A., Ortiz-Monasterio, I., Rahn, T., & Griffith, D. W. (2001). Identifying the agricultural imprint on the global N_2O budget using stable isotopes. *Journal of Geophysical Research: Atmospheres*, *106*, 9869–9878.

Prather, M. J., Holmes, C. D., & Hsu, J. (2012). Reactive greenhouse gas scenarios: Systematic exploration of uncertainties and the role of atmospheric chemistry. *Geophysical Research Letters*, *39*(9) https://doi.org/10.1029/2012GL051440

Prather, M. J., Hsu, J., DeLuca, N. M., Jackman, C. H., Oman, L. D., Douglass, A. R., et al. (2015). Measuring and modeling the lifetime of nitrous oxide including its variability. *Journal of Geophysical Research: Atmospheres*, *120*, 5693–5705. https://doi.org/10.1002/2015JD023267

Prokopiou, M., Martinerie, P., Sapart, C. J., Witrant, E., Monteil, G., Ishijima, K., et al. (2017). Constraining N_2O emissions since 1940 using firn air isotope measurements in both hemispheres. *Atmospheric Chemistry and Physics*, *17*, 4539–4564. https://doi.org/10.5194/acp-17-4539-2017

Prokopiou, M., Sapart, C. J., Rosen, J., Sperlich, P., Blunier, T., Brook, E., et al. (2018). Changes in the isotopic signature of atmospheric nitrous oxide and its global average source during the last three millennia. *Journal of Geophysical Research: Atmospheres*, *123*, 10757–10773. https://doi.org/10.1029/2018JD029008

Rahn, T., & Wahlen, M. (1997). Stable isotope enrichment in stratospheric nitrous oxide. *Science*, *278*, 1776–1778. https://doi.org/10.1126/science.278.5344.1776

Rahn, T., & Wahlen, M. (2000). A reassessment of the global isotopic budget of atmospheric nitrous oxide. *Global Biogeochemical Cycles*, *1*, https://doi.org/10.1029/1999GB900070. issn: 0886–6236.

Ravishankara, A. R., Daniel, J. S., & Portman, R. W. (2009). Nitrous oxide (N_2O): The dominant ozone-depleting substance emitted in the 21st century. *Science*, *326*, 123–125. https://doi.org/10.1126/science.1176985

Ray, E. A., Portmann, R. W., Yu, P., Daniel, J., Montzka, S. A., Dutton, G. S., et al. (2020). The influence of the stratospheric Quasi-Biennial Oscillation on trace gas levels at the Earth's surface. *Nature Geoscience*, *13*, 22–27. https://doi.org/10.1038/s41561-019-0507-3

Reinecker, M. M., Suarez, M. J., Todling, R., Bacmeister, J., Takacs, L., Liu, H.-C., et al. (2008). *The GEOS-5 data assimilation system-documentation of versions 5.0.1, 5.1.0, and 5.2.0, Tech. Rep. 104606 V27*, NASA.

Röckmann, T., Kaiser, J., & Brenninkmeijer, C. A. M. (2003). The isotopic fingerprint of the pre-industrial and the anthropogenic N_2O source. *Atmospheric Chemistry and Physics*, *3*, 315–323. https://doi.org/10.5194/acp-3-315-2003

Röckmann, T., & Levin, I. (2005). High-precision determination of the changing isotopic composition of atmospheric N_2O from 1990 to 2002. *Journal of Geophysical Research: Atmospheres*, *110*, D21304. https://doi.org/10.1029/2005JD006066

Saikawa, E., Prinn, R. G., Dlugokencky, E., Ishijima, K., Dutton, G. S., Hall, B. D., et al. (2014). Global and regional emissions estimates for N_2O. *Atmospheric Chemistry and Physics*, *14*, 4617–4641. https://doi.org/10.5194/acp-14-4617-2014

Saikawa, E., Schlosser, C. A., & Prinn, R. G. (2013). Global modeling of soil nitrous oxide emissions from natural processes. *Global Biogeochemical Cycles*, *27*. https://doi.org/10.1002/gbc.20087

Snider, D. M., Venkiteswaran, J. J., Schiff, S. L., & Spoelstra, J. (2015). From the ground up: Global nitrous oxide sources are constrained by stable isotope values. *PLoS One*, *10*(3), e0118954. https://doi.org/10.1371/journal.pone.0118954

Sowers, T., Rodebaugh, A., Yoshida, N., & Toyoda, S. (2002). Extending records of the isotopic composition of atmospheric N_2O back to 1800 A.D. from air trapped in snow at South Pole and the Greenland Ice Sheet Project II ice core. *Global Biogeochemical Cycles*, *16*(4), 1129. https://doi.org/10.1029/2002GB001911

SPARC. (2013). The lifetimes of stratospheric ozone-depleting substances, their replacements, and related species. *SPARC Rep*. 6, WCRP-15/2013, eds. In M. Ko (Ed.), et al., SPARC Office.

Thompson, R. L., Ishijima, K., Saikawa, E., Corazza, M., Karstens, U., Patra, P. K., et al. (2014). TransCom N_2O model inter-comparison, Part II: Atmospheric inversion estimates of N_2O emissions. *Atmospheric Chemistry and Physics*, *14*, 6177–6194. https://doi.org/10.5194/acp-14-6177-2014

Thompson, R. L., Lassaletta, L., Patra, P. K., Wilson, C., Wells, K. C., Gressent, A., et al. (2019). Acceleration of global N_2O emissions seen from two decades of atmospheric inversion. *Nature Climate Change*, *9*, 993–998. https://doi.org/10.1038/s41558-019-0613-7

Tian, H., Xu, R., Canadell, J. G., Thompson, R. L., Winiwarter, W., Suntharalingam, P., et al. (2020). A comprehensive quantification of global nitrous oxide sources and sinks. *Nature*, *586*, 248–256. https://doi.org/10.1038/s41586-020-2780-0

Toyoda, S., Kuroki, N., Yoshida, N., Ishijima, K., Tohjima, Y., & Machida, T. (2013). Decadal time series of tropospheric abundance of N_2O isotopomers and isotopologues in the Northern Hemisphere obtained by the long-term observation at Hateruma Island, Japan. *Journal of Geophysical Research: Atmospheres*, *118*, 3369–3381. https://doi.org/10.1002/jgrd.50221

Toyoda, S., Yoshida, N., Urabe, T., Nakayama, Y., Suzuki, T., Tsuji, K., et al. (2004). Temporal and latitudinal distributions of stratospheric N_2O isotopomers. *Journal of Geophysical Research*, *109*, D08308. https://doi.org/10.1029/2003JD004316

Wofsy, S. C. (2011). The HIPPO Science Team and Cooperating Modellers and Satellite Teams, HIAPER Pole-to-Pole Observations (HIPPO): Fine-grained, global-scale measurements of climatically important atmospheric gases and aerosols. *Philosophical Transactions of the Royal Society A*, *369*, 2073–2086. https://doi.org/10.1098/rsta.2010.0313

Yoshida, N., & Toyoda, S. (2000). Constraining the atmospheric N_2O budget from intramolecular site preference in N_2O isotopomers. *Nature*, *405*, 330–334. https://doi.org/10.1038/35012558

Yu, L., Harris, E., Henne, S., Eggleston, S., Steinbacher, M., Emmenegger, L., et al. (2020). The isotopic composition of atmospheric nitrous oxide observed at the high-altitude research station Jungfraujoch, Switzerland. *Atmospheric Chemistry and Physics*, *20*, 6495–6519. https://doi.org/10.5194/acp-20-6495-2020

Yung, Y. L., & Miller, C. E. (1997). Isotopic fractionation of stratospheric nitrous oxide. *Science*, *278*, 1778–1780. https://doi.org/10.1126/science.278.5344.1778